Synthesis and Characterization of $Ce_xTi_{1-x}O_2$ Nanostructures

by

VarunSama

Submitted in Partial Fulfillment of the Requirements

for the Degree of

Master of Science in Chemistry

YOUNGSTOWN STATE UNIVERSITY

August, 2013

ETD Program

Digitally signed by ETD Program
DN: cn=ETD Program, o=School of Graduate Studies and Research, ou=Youngstown State University, email=etdadmin@cc.ysu.edu, c=US
Date: 2013.09.24 10:15:40 -04'00'

SIGNATURE PAGE

I hereby release this thesis to the public. I understand that this thesis will be made available from the OhioLINK ETD Center and the Maag Library Circulation Desk for public access. I also authorize the University or other individuals to make copies of this thesis as needed for scholarly research.

Signature:

VarunSama, Student Date

Approvals:

Dr. Ruigang Wang, Thesis Advisor Date

Dr. Timothy R. Wagner, Committee Member Date

Dr. Sherri Lovelace Cameron, Committee Member Date

Dr. Bryan DePoy, Interim Dean of School of Graduate Studies and ResearchDate

ABSTRACT

The basic function of vehicle three way catalytic converters is to convert the harmful exhaust pollutant gases (CO, NO_x, and unburned hydrocarbons) to less harmful gases, for example, from carbon monoxide to carbon dioxide. But this conversion occurs at relative high temperature. The purpose of this study is to synthesize low-temperature catalytically active wash coat oxide nanomaterials for vehicle catalytic converters, via a hydrothermal reaction method. Various characterization techniques such as powder X-ray diffraction, thermogravimetric analysis, temperature programmed reduction, BET surface area measurement, and transmission electron microscopy were used for the analyses of the synthesized nanopowders. We found that the sample with nanotube morphology showed superior low-temperature performance compared to other morphology nanoparticles. The mechanism for this improved low-temperature activity in CeO_2-TiO_2 nanotubes will be discussed.

ACKNOWLEDGEMENTS

I am greatly thankful to my advisor Dr.Ruigang Wang for his support, motivation, patience and the immense knowledge he imparted on me was very crucial, which helped me in completing the thesis as robust as possible.

I would like to thank my committee members Dr. Sherri Lovelace-Cameron and Dr. Timothy R. Wagner for their time and valuable suggestions on my thesis.

I wish to thank Dr. Timothy R. Wagner and Dr. Josef Simeonsson for the use of their equipment. I would like to thank Dr. Matthias Zeller for helping me in characterizing the XRD data.

I would like to thank my parents for their support and blessings. I would like to thank my lab mate Samuel Mutinda for his help. I would like to thank my friends Vamshi Inumula, Ramesh Gondi and Sandeep Kakkerla for their support.

Last but not least, I would like to thank Department of Chemistry, School of Graduate Studies, ACS-PRF (grant # 52323), DoT CTME projectfor the financial support.

TABLE OF CONTENTS

List of Tables

Table of Figures

Chapter 1 Introduction

In the past 50 years the application of nanomaterials has increased widely and they rendered huge profits for the companies. The importance to the nanomaterials increased because the properties of the bulk materials and nanomaterials of the same composition varied a lot with a much enhanced surface area. Surface effect is key factor for the nanomaterials. Nanomaterials have larger surface to volume ratio compared to the bulk materials. Materials with nanoscale structures are found to exhibit high reactivity because of their typical atomic re-arrangements on the surface, and the dangling bonds due to the presence of the fewer number of nearest atoms, which causes shortening of the bond distances between the bulk and surface atoms [1]. In thesis, we studied the synthesis and catalytic property of cerium titaniummixed oxides, which have many important industrial applications, such as in three-way catalyst, fuel cells, water-gas shift reactions etc.

1.1CeO_2 used as catalyst

The most important application regarding the ceria, also called cerium oxide (CeO2), is its active role in the three way catalyst (TWC) for automotive catalytic converter. Ceria exhibits catalytic activity because of their ability to switch between the +3 and +4 states very easily [2]. Ceria when treated at elevated temperatures in reducing atmosphere yields a well-known continuum of oxygen-deficient, non-stoichiometric CeO_{2-x} oxides ($0 \leq x \leq 0.5$) and in lower temperatures ($T < 450\ ^{o}C$) it showed a series of discrete compositions and the best part of the ceria is even after the loss of the significant number of lattice oxygen it still retains its fluorite structure and easily retains its oxygen once exposed to the oxygen atmosphere for a short period of time [3]. The

reduction behavior of the ceria can be analyzed by exposing it to H_2 or CO. These results can be best analyzed by using temperature program reduction (TPR). In the automotive three-way catalytic converters, carbon monoxide is the major pollutant. Cerium oxide helps reacts with the carbon monoxide and helps in its conversion to carbon dioxide. The following reaction usually takes place between cerium oxide and carbon monoxide.

$$2\ CeO_2 + CO \longrightarrow Ce_2O_3 + CO_2$$

$$2\ Ce_2O_3 + O_2 \longrightarrow 4\ CeO_2$$

The TPR results yields two peaks one of them will be at low temperature that is due to surface reduction and the other one will be at higher temperature and that is due to the bulk reduction that is removal of bulk oxygen. The lowest peak usually showed at 497 ^oC and the one with highest temperature indicated at 827 ^oC. Several researchers tried to reduce this surface and bulk reduction temperatures to considerably lower level for long lasting product activity. Ceria also has lot of applications in different fields and some of them are given in Table 1.

Table 1: Application of cerium oxide

Application examples	References
Fuel cells	[9,10]
Insulators	[10]
UV blockers	[11]
Polishing materials	[12-14]
Gas sensors	[12]

1.2 Crystal structures:

Cerium oxide (CeO_2):

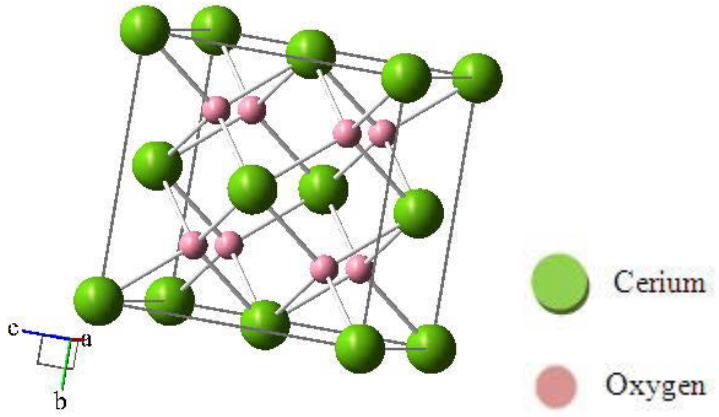

Figure 1:Crystal structure of cerium oxide

As shown in Figure 1, ceria exhibits face-centered cubic fluorite structure. With increase in the oxygen vacancy, the activity of ceria increases as the space in the lattice increases which will make ceria to reduce and oxidize very easily. The catalytic activity of the ceria is directly related to this property. The optimum catalytic activity of ceria is based on its crystal structure typical arrangement of the oxygen atoms around the cerium ions.

Ceria (CeO_2) in general is oxidized product of the cerium metal. Cerium is one of the most abundant rare earth metals and is easily oxidized to form cerium oxide. It is ductile, soft, and silvery and it belongs to the lanthanide group. Cerium is given importance because of its easily oxidizing nature and also its typical electronic structure(dual valence state: +3 and +4). Cerium oxidizes readily at 150^{o}C to form cerium oxide. Cerium because of its higher electropositive nature reacts slowly with cold water and quite quickly with hot water to form cerium hydroxide. The most commonly and frequently formed compound of the cerium is cerium oxide (ceria, CeO_2). Many

researchers synthesized cerium oxide using different synthesis techniques. For example, T.masui et al. synthesized ceria nanoparticles by the conventional hydrothermal methods employing tetravalent cerium salts $Ce(SO_4)_2$,$Ce(NH_4)_4(SO_4)_2$,and $(NH_4)_2Ce(NO_3)_6$) as starting materials [7].Masanori Hirano et al. carried out the synthesis using hydrothermal technique by using cerium sulfate tetra hydrate, cerium ammonium sulfate dehydrate, and urea as starting materials.

Titanium oxide (TiO_2):

Titania (TiO_2) usually exists in a lot of crystalline forms but the most predominant among them is the Rutile and Anatase phases. Of the entire existing forms major share is of rutile followed by anatase and others [4]. Titanium oxide has eight modifications in addition to its rutile, anatase and brookite forms. Rutile phase is most predominant than the other two phases. Rutile phase exhibits high dispersion and also has the highest refractive indices of any known mineral. Rutile in its natural form contains 10% iron and traces of niobium and tantalum. Figure 2 shows the tetragonal structures of rutile and anatase phase titanium oxide.

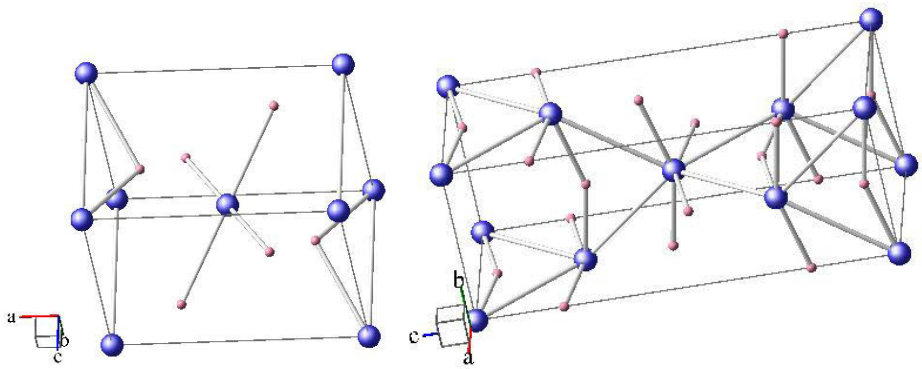

(a) (b)

Figure 2: Crystal structure of (a) Rutile and (b) Anatase phase titanium oxide

Thermodynamically, rutile is the most stable polymorph of TiO_2 at all temperatures. Transformation of rutile to anatase phase is irreversible. All three major polymorphs of titania exhibit a same structural similarity. They have tetragonal structure but the major difference is only unit cell parameters. The unit cell parameters of rutile phase are a, b=4.59 Å, c=2.95 Å, and the unit cell parameters of anatase phase are a, b=3.78 Å, c= 9.51 Å. The symmetry and arrangement of atoms in rutile phase is much systematic and evenly arranged compared to the random arrangement of atoms in anatase phase. Due to this the anatase phase is not stable even at lower temperatures and readily transforms to rutile phase. The synthesis of anatase phase is easier than rutile phase [5]. Anatase has the same structural properties as of the rutile and brookite except the interfacial angles of the two minerals. At around 550 ^{o}C to 1100 ^{o}C anatase will be transformed to most stable rutile phase with an increase in the specific gravity to 4.2 and this is why it is considered as not an equilibrium phase of titanium dioxide.

Pure titanium oxide received a lot of attention due to its chemical stability, non-toxicity, low cost and other advantages. The most important application of the titanium dioxide is it is used as pigment, photo catalyst. The other applications include UV absorber and electronic data storage medium.

Perovskite cerium titanium oxide ($CeTiO_3$):

The most common forms of cerium titanium mixed oxide that were synthesized earlier are $CeTiO_3$ (Perovskite) and $CeTi_2O_7$(Pyrochlore). The perovskite form is more stable and can be easily synthesized. Figure 3 shows typical orthorhombic structure of perovskite cerium titanium oxide.Thermal treatment of perovskite $CeTiO_3$ can transform it into rutile or anatase phase.

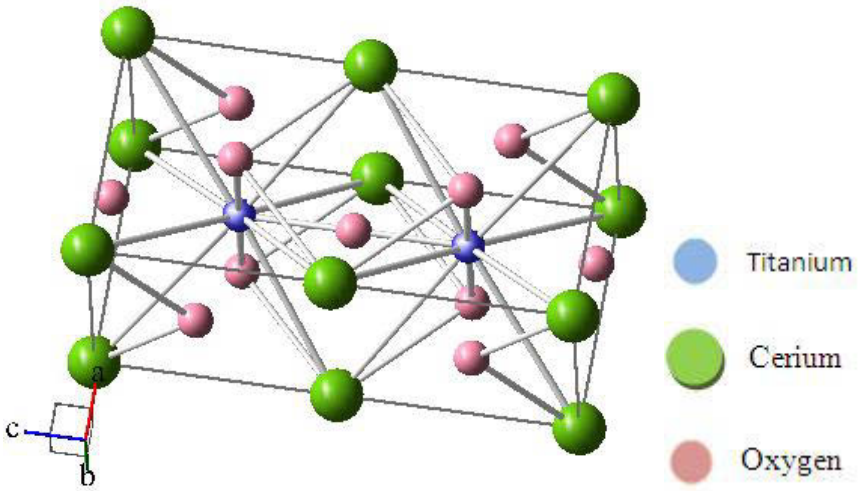

Figure 3: Crystal structure of perovskite $CeTiO_3$

1.3 Cerium based mixed oxide:

Cerium oxide is a well-known additive in the automotive three way catalysts. Pure cerium oxide exhibits poor thermal stability and undergoes sintering at high temperatures, thus greatly decreasing its oxygen storage capacity [6].

The catalytic activity of ceria can be enhanced by doping with other metal oxides. Generally, doping of ceria with other metal oxides results in the introduction of oxygen vacancies in the crystal without adding any electronic charge carriers. This results in the

enhanced ionic conductivity. Modifying ion stability inside the ceria lattice by replacing the cerium ions by ions of different charge and size yields a distorted lattice ceria structure, which enhances various properties of the ceria; some of them present improved thermal stability against sintering at higher temperatures and enhanced catalytic activity. Table 2 shows various cerium based mixed oxides synthesized earlier by different techniques.

Most of the mixed oxides shown in the Table 2 have been tested for auto exhaust catalysis or three way catalysts and also in oxygen sensors. It has been reported that the cerium-based mixed oxides present superior oxygen storage capacity under oxygen rich and lean conditions.

Table 2: Comparison of the synthesis method, BET surface area, reduction temperature of cerium oxide based mixed oxides

Mixed oxide	Synthesis technique	BET surface area (m^2/g)	Reduction temperature (^oC)	References
$Ce_{1-x}Ca_xO_2$	Microemulsion	130	527	[1]
$Ce_{1-x}Tb_xO_y$	Microemulsion	121	506	[2]
$Ce_{1-x}Ba_xO_2$	Distillation	-	627	[3]
$CeNi_xO_y$	Coprecipitation	-	544	[4]
$CeCu_xO_y$	Coprecipitation	-	564	[4]
$Ce_xMn_yO_z$	Decomposition	38	700	[5]
$Ce_{1-x}Zr_xO_2$	Precipitation	-	580	[6]
$Ce_1Ti_{1-x}O_2$	Hydrothermal	120	466	In this study

1.4 Cerium titanium mixed oxides:

Ceria doped with zirconium oxide (ZrO_2), hafnium oxide (HfO_2) or other rare earth metal oxides (PrO_2, TbO_2) has been studied intensely because they exhibit better low-temperature reducibility and superior thermal stability. Ionic radius is one of the important factors for the formation of mixed oxides or oxide solid solutions, as smaller ions can easier substitute larger ions and form solid solution. Ionic radius of titanium is lower than that of zirconium and hafnium, shown in Table 3. Many researches earlier stated that mixing titanium oxide with cerium oxide or vice versa can enhance the catalytic properties and thermal stability due to structural modification and change in electronic properties. In this thesis, we prepared a series $Ce_xTi_{1-x}O_2$ ($0 \leq x \leq 1$) using two different methods in order to study the doping effect on the catalytic activity in the mixed oxides.

Table 3: Ionic radius of various elements

Element	Ionic Radius (Å)
Cerium	0.97
Zirconium	0.79
Hafnium	0.78
Titanium	0.64

Various methods have been reported to synthesize cerium titanium mixed oxides. Some of them were shown in the Table 4 below.

Table 4:Different methods of synthesis of cerium titanium mixed oxideDifferent methods of synthesis of cerium titanium mixed oxide

Synthesis method	Particle size (nm)	BET surface area (m^2/g)	References
Sol-gel	5.95	-	[9]

Precipitation	5.4	119.2	[10]
Sol-gel	5	105	[11]
Sol-gel	55	126.1	[12]
Impregnation	18.4	72.6	[12]
Coprecipitation	7.2	53.8	[12]

Cerium titanium mixed oxides have been reported as playing an important role in heterogeneous catalysis, electrochemistry, gas sensors, and corrosion /wear protection, etc.

CHAPTER 2:Hydrothermal synthesis and instrumentation

In this chapter two topics were discussed. One is regarding the hydrothermal synthesis technique that is used in our project to synthesize $Ce_xTi_{1-x}O_2$ ($0 \leq x \leq 1$) nanostructures and the second one is regarding the instruments and techniques that we used for characterizing the materials.

2.1 Hydrothermal synthesis:

There are many synthesis techniques like sol-gel synthesis, sonochemical synthesis, reverse micellar synthesis, microwave-hydrothermal synthesis techniques that are very predominant in the synthesis of the pure cerium oxide, pure titanium oxide and cerium titanium mixed oxide but the one that is used in our project is hydrothermal synthesis. Morphology of particles can be controlled using this hydrothermal synthesis and the particles with good catalytic properties can also be synthesized using this technique.

Hydrothermal synthesis is a typical process that usually takes place at a very high vapor pressure and also at high temperatures (above 100 ^oC). Morey and Niggli [23] defined that this method uses above critical temperature of water for the synthesis. Laudise [24] stated that the synthesis occurs at ambient or near ambient conditions and according to Rabenau [25] reaction takes place at 100 ^oC and a pressure of 1 bar According to Yoshimura [26] the hydrothermal synthesis is the technique that takes place under high temperature that is above 100 ^oC and at high pressure that is above 1 Mpa in the aqueous medium in closed system. Finally from all the above definitions it can be

defined as the reaction that is occurring above 100 ^{o}C and above 1 Mpa. But in the recent days the synthesis was performed even under 100 ^{o}C. So, due to this it can be redefined as any heterogeneous reaction that is occurring above 1 Mpa pressure and above room temperature. In general the synthesis conducted above 200^{o}C considered as severe conditions and the synthesis conducted below that temperature are considered as mild conditions. The synthesis done at mild conditions found to be a break through step in this hydrothermal technique. The pressure at that temperature was less than 1.5 Mpa. In this hydrothermal synthesis even the solvents which are insoluble at normal conditions will be dissolved and form complexes. The major reactions that occur by this technique are synthesis of new phase compounds, crystal formation of most of the inorganic materials and so on. In the past few years the importance of hydrothermal synthesis has increased a lot and the major reason for that it helped to study the effect of individual parameters that include temperature, pressure and compositional effects during the synthesis of new phase compounds. The product obtained from the hydrothermal synthesis will be very pure, finely grinded without any agglomerations, any hazardous waste can be decomposed without any pollution, noise free, and the most important aspect is the production of new phase compounds with low power consumption and it don't require any kind of expensive or highly sophisticated equipment.

Principle in hydrothermal synthesis is the production of nanocrystalline inorganic materialsat an elevated temperature and pressure in a direct precursor to product mechanism and it does not use any product directing agents by dissolving almost all the inorganic substances in the water.The three important principle physical parameters in

hydrothermal synthesis are temperature, water vapor pressure and time of reaction. In this process water vaporization at elevated temperature plays a key role.

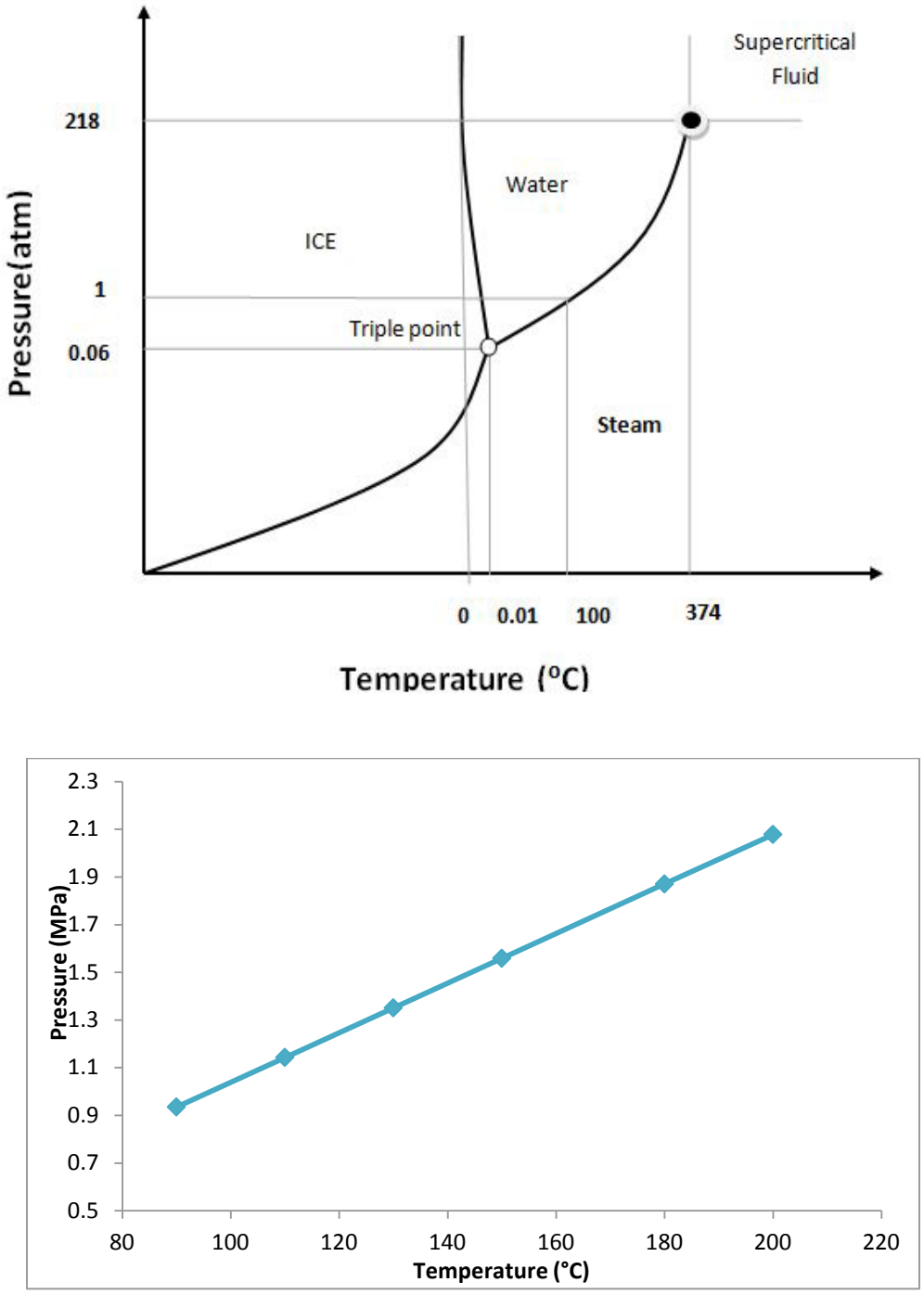

Figure 4: Phase diagram of water and hydrothermal synthesis

Phase diagram of water (Figure 4) gives better understanding of this synthesis technique [27]. In the hydrothermal synthesis the phase between liquid and gas is the key point for the synthesis of novel compounds even under lower temperatures (below 180 ^{o}C) compared to other techniques. Because below 100 ^{o}C the pressure remains less than 1 Mpa but above that temperature the pressure that is necessary for the synthesis will be available. For this hydrothermal synthesis elevated vapor pressure is used instead of equilibrium vapor pressure. The main reason behind using the elevated vapor pressure is because the solubility of the inorganic materials will be very high at high pressures [24-26]. There are usually two techniques for the synthesis of nanoparticles. One is top down technique and the other one is bottom up technique (Figure 5). In the top down technique nanoparticles are synthesized from the bulk materials. Here bulk material will break down into smaller particles gradually and finally nanoparticles are obtained. In the second technique smaller particles build up or combine into clusters and form nanoparticles [28]. Both the techniques are very important in the synthesis of nanomaterials. In our project we used hydrothermal method, which is a bottom up technique.

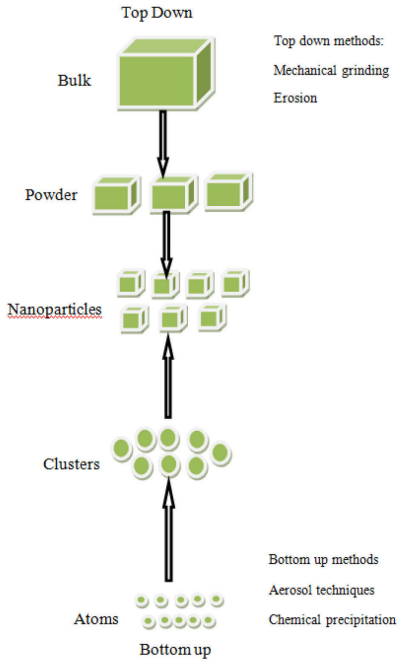

Figure 5: Schematic representation of synthesis of nanomaterials

Figure 6: Components of hydrothermal synthesis devices and a temperature programmedfurnace

Figure 6 shows the components of hydrothermal synthesis. The autoclave shown in the figure was used to load the samples. It is resistant to high pressure and temperature and also inert. Its resistance is due to teflon coating. This autoclave is placed in stainless steel shell and then it is transferred to temperature programmed furnace for further reaction.

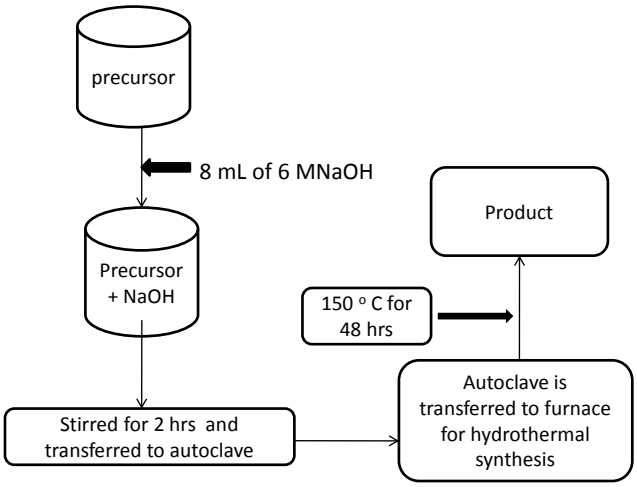

Figure 7: Schematic of Hydrothermal synthesis

Synthesis can be done based on segment system using this programmable furnace. For our research we used 4 segment system and each segment has its own function. In the 1st segment temperature was raised to the target temperature at a rate of 10 ^{o}C/min. In the second segment the sample was kept constant at the target temperature for target time. The pressure for this synthesis at 150^{o}C was 1.5 Mpa. The pressure involved in the hydrothermal reaction was calculated using Clapeyrons equation

$$PV = nRT \qquad (1)$$

Here P = Pressure that we need to calculate

V = Volume that we fill in the autoclave

n = Number of mols of the reactants

R = Gas constant

T = Temperature that we used for the hydrothermal reaction

The pressure varies with filling volume of the autoclave and also the temperature. In our synthesis we usually fill the autoclave to 45 %. So, for that temperature and to that filling volume the pressure was 1.5 Mpa and the dwell time that we used for precipitation method was 48 hours and the dwell time used for nanotube template method was 72 hours and in the 3rd segment the temperature was cool down to room temperature with a cooling rate of 10 ^{o}C/min and the final segment was termination of the process.

The advantages of hydrothermal method are that crystalline, amorphous or anhydrous powders can be synthesized directly from the solutions. It is possible to control particle size, particle shape and chemical composition and it is suitable for the synthesis of metastable structures [29]. Most of the products synthesized with this process do not need calcination and they are highly crystallized.

2.2 Instrumentation and characterization Techniques:

In this project various instruments were used for the sample characterization and that include, powder X-Ray diffraction (P-XRD), thermogravimetric analysis (TGA), temperature programmed reduction (TPR), BET surface area measurement, transmission electron microscopy (TEM) and Raman spectroscopy. Powder X-ray diffraction was used to determine crystal structure and crystallite size; Temperature programmed reduction

was used to analyze the reduction temperature, hydrogen consumption,and also determines the heterogeneity of reducible surface; BET was used to analyze the specific surface area of the materials;TEM was used to determine morphological and crystallographic information of the samples up to atomic level and finally Raman spectroscopy was used to determine the vibrational, rotational and other low frequency modes of a compound.

2.2.1 Powder X-ray diffraction (PXRD):

The XRD is of mainly two types: single crystal X-ray diffraction and powder X-ray diffraction.In case of analyzing single crystalline samples, the sample should be a perfect crystal with a cross section of 0.3 mm. These single crystal XRD is mainly used to analyze the molecular structures of novel compounds. In case of analyzing the powder sample, it should be arranged very flat and should and evenly distributed on the sample holder and this technique is employed to identify finger print identification of the compounds.

In both the analysis the sample should be smoothly dispersed onto the sample holder. The X-ray from the X-ray tube will be out and the divergent slit will scatter the rays onto the sample. The reflected rays will be collected by the detector. When the particles interact with the oncoming X-rays the rays get diffracted and finally get a diffraction pattern that is obtained from the detector. That is the reason why X-ray pattern of a pure substance is considered as a fingerprint of its own and this property made powder XRD as suitable technique to analyze both powder samples and polycrystalline samples [31].

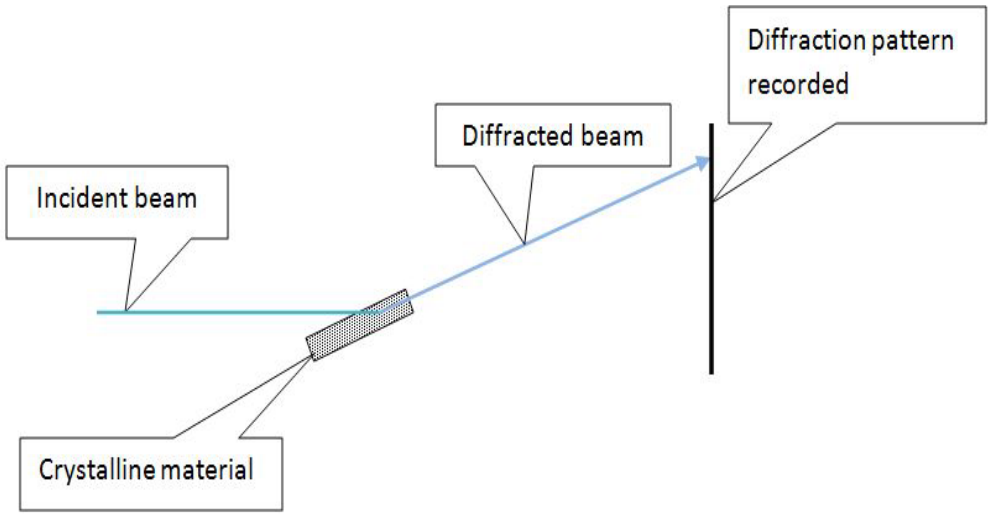

Figure 8: Basic schematic of X-ray diffraction

Figure 8 shown above clearly explains the basic principle involved in the X-ray diffraction. The principle here is when an "X-ray (incident beam) hits an atom (crystalline material) the energy will be transferred to the electrons and that electrons around the atom they start to oscillate with the frequency of the beam that hit the atom and the transmitted rays will further have destructive interference in almost all directions [32]. The transmitted rays (diffracted beam) will be collected using the detector. These collected rays will be useful to analyze the crystal structure of the material.

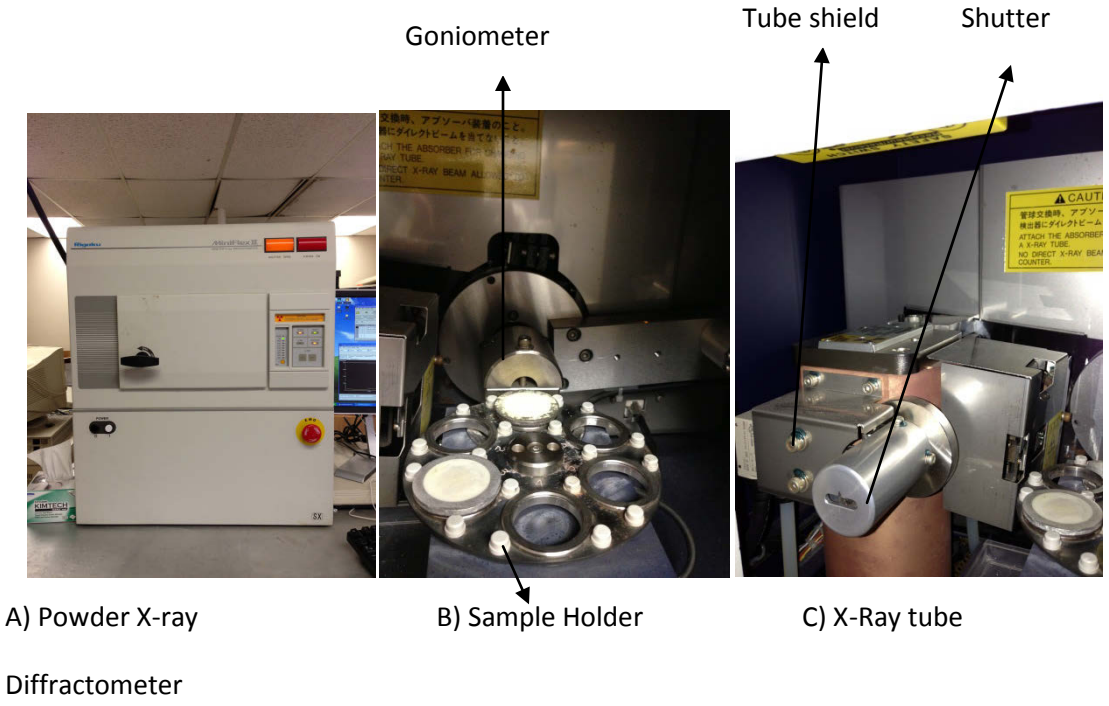

D) Detector

Figure 9: Components of powder X-ray diffractometer (Rigaku)

Figure 9 shows the different components of Rigaku X-ray diffraction which we used in our study.One of the important parts of the XRD is goniometer and its assembly includes 3 parts; sample holder, detector arm and its associated gearing. The sample holder used for the analyses was made of aluminum and the wavelength of the incident X-ray beam was 1.5406 Å. The amount of sample required for analyses is about 0.9 g. The scan rate that we used was 0.5 ^{o}/min and the scan range was from 10-90^{o}. The distance between the X-ray focal spot to the sample should be same as the distance

between the sample holder and detector. There are two kinds of setup for the goniometer one is the most popular 2-Theta-Theta setup and the other one is Theta-Theta setup. In the former one the sample holder will bend according to the final target angle. In this case the sample should be prepared very well if the sample is loosely packed and if the final target angle is more the sample may fall from the holder. In case of later one both detector and the X-ray tube will bend according the target theta and the sample holder remains constant. The standard focal spot for any kind of X-ray tube is 10 mm long and 1 mm wide. It is mandatory to maintain the focusing distance constant at all times by maintaining the ratio between the sample and the detector. The diffraction patterns will be obtained using reflected patterns versus detector angle.

Bragg's Equation is employed for the identification of the d-spacing as shown in Equation 2.

$$2d\sin\theta = n\lambda \quad (2)$$

Where *d* is the spacing between the planes in the atomic lattice; θ is the angle between the incident ray and the scattering planes; λ is the wavelength of the incident X-ray beam (Cu k_α 1.5406 Å); n is an integer.

The crystallite size of nanoparticles is calculated using Scherrer equation which is shown below Equation 3

$$r = \frac{K\lambda}{\beta cos\theta} \quad (3)$$

Where r is the crystallite size; K is a constant and the value used is 0.9 for the calculations; λ is the wavelength of radiation source (1.5406 Å); βis the peak full width at half maximum(FWHM); and θ is angle of reflection.

XRD have wide range of applications. But the one that are in particular to our project are it is helpful in identification of crystal structure of unknown samples and also varied number of compounds can be identified by a simple search match procedure. Crystallite size and shape can be measured using this characterization. It is also helpful in the identification of different phases of a compound, solid solutions and unit cell parameters and also Identification of crystalline nature of polymers

2.2.2 Temperature programmed reduction (TPR) and BET surface areameasurement:

TPR is generally used to find the most efficient reduction temperatures of the inorganic solid materials and is often used in the field of heterogeneous catalysis. The sample is loaded in the simple quartz glass container that is called as U-tube which is positioned in the furnace with temperature control equipment (see Figure 10). A thermocouple is placed close to the solid sample to measure the temperature. The air that is already inside the U-tube sample holder is removed using inert gases such as argon. Pretreatment was done for at least1 hour by passing the argon gas through the sample to create inert atmosphere inside the U-tube.

TPR is a chemisorption technique and it involves in chemical reactions between surface of the compound and the adsorbate. At the adsorbate new chemical bonds are synthesized [33]. The temperature where the sample gets reduced will be accurately measured by the thermocouple andthe composition of the gaseous mixture is measured at

the exit of the sample container with thermal conductivity detector (TCD) based on the difference in thermal conductivity of the purge gas and resulting gases. This technique is used for the chemical characterization of the solid material to determine the reduction temperature and also used in heterogeneous catalysis to test the reactivity of catalysts. This technique is highly sensitive. The instrument operating is very easy with simple programmers. Every peak obtained will have its characteristics relating to the sample chemical nature.

A) Temperature program reduction B) Cold trap to remove condensable species.

C) Clamshell Furnace Thermocouple D) Sample Tube (U - tube)

Figure 10: Components of Micromeritics Autochem II 2920 instrument

Micromeritics Autochem II 2920 is equipped with highly sensitive thermocouple detector and it also contains four high precision mass flow controllers that help to attain most accurate gas control. It has detector elements that are corrosion resistant which can resist most of the destructive gases. It also has a clamshell furnace which can resist and treat sample up to 1100^{o}C and finally the important feature of this instrument is it has four carrier gas inlets, four loop gas permits and four preparation gas inlets.

In our research we used U-tube to load the samples and that tube is made of quartz glass, which can tolerate high temperature usage. The quantity of sample that we used was ranging from 0.05 g to 0.08 g. The sample was sandwiched between glass wool to avoid the loss of sample from the tube. We did pretreatment for the sample by flowing argon gas at a rate of 50 mL/cm^3 at 110 ^{o}C for 1 hour. Once it is done we usually do BET analysis and then TPR analysis. The reason for that is the TPR analysis will be done up to 950 ^{o}C and due to this high temperature the sample gets destroyed and cannot be used for further analysis. For BET analysis we use pure nitrogen and for TPR we hydrogen argon mixture (5%H_2/95%Ar).The highest temperature that we use for the TPR analysis was 950 ^{o}C and the heating rate was adjusted to 10 ^{o}C/min. The gas flows through the sample tube (U-tube). The unreacted gas will exits out of the tube. In the beginning the gas entering the analyzer is equal to the gas flowing onto the detector. Once the sample reaches the critical temperature it will react with the gas mixture and forms water molecules ($4CeO_2+H_2 \rightarrow 2Ce_2O_3+H_2O$). These water molecules are removed from the gas stream. The formation of water molecules will continue until there is no more hydrogen gas in the mixture. If there is no more hydrogen gas in the gas mixture there will be no

more reaction taking place due to the lower conductivity of the argon gas [34]. This difference is identified by the thermal conductivity detector.

It is helpful in the identification of reduction temperature of the materials and the amount of sample required for the analysis is much less. But the problem with TPR analysis is the sample is not reusable because the reaction is carried out at very high temperature and at that temperature the sample was completely destroyed.

BET surface area measurement:

BET method is used to analyze the surface area of the particles. The surface area of the particles can be calculated by the physisorption that is physical adsorption of the gas molecules on the solid surface. BET is purely based on the multilayer adsorption mechanism which is an extension of the monolayer concept of the Langmuir isotherm mechanism. The surface area can be calculated using the amount of the gas adsorbed by the sample molecules.

Physisorption or physical adsorption is the principle mechanism of BET. This technique is employed for the determination of specific surface area of the desired powder sample. The surface area can be determined by the physical adsorption of the gas on the solid surface of the powder sample. Nitrogen gas is used generally for the determination and liquid nitrogen (Temperature: 77 K) is kept over the sample to maintain the temperature.

The determination is carried out at the liquid nitrogen temperature. Nitrogen is used usually because of its high purity in nature and strong interaction. Due to its low temperature the gas adsorbs very easily onto the solid surface [35]. The interaction forces

that results in physical adsorption are vanderwaals forces and this interaction are very weak. The nitrogen gas is released in known amounts stepwise and this nitrogen is adsorbed onto the surface of the sample and the rest of the gas that is unabsorbed will be detected by the detector and this gives the final result displayed on the screen.

BET surface area can be calculated using the following equation 4

$$\frac{1}{W[(P_O/P)-1]} = \frac{1}{W_m C} + \frac{C-1}{W_m C}\frac{P}{P_O} \qquad (4)$$

Here P/P_o is relative pressure of the gas, C is constant, X and $X_m$are related to surface area

Before starting the analyzation of the surface area it is recommended to perform pretreatment to remove any gases if present around the sample. In the pretreatment inert gas like helium is passed through the sample for a minimum time period of 1hour at 110 ^oC and creates inert atmosphere around the sample. This ensures the determination of surface area to the maximum possible point.The experiment is conducted at a relative pressure which is lower than the atmospheric pressure. This lower relative pressure is attained by partial vacuum. After the saturation pressure point no more adsorption occurs and the process stops automatically. The BET isotherm is the plot of the collected data. The isotherm is plotted using amount of gas adsorbed versus relative pressure.

2.2.3 Thermogravimetric analysis (TGA):

Thermogravimetric analysis is a technique used to characterize materials by monitoring the weightchange of a substance as a function of temperature. Thermal stability of the compound and fraction of volatile components in a compound can be

identified by this analytical technique by change in the weight of the sample. There can be decrease in the sample weight due to heating or increase at the time of cooling and this change in the weight of the sample is used to analyze the sample. The analysis is carried out mostly in the inert atmosphere and the gases used are helium or argon.

The most important part of TGA is the sample pan which contains a precision balance and the sample in this pan will be heated or cooled based on the type of experiment and the sample atmosphere is maintained using inert gases or reactive gases. The gas is flowed through the sample and exits through an exhaust. There are two types of TGAs, one is with arrangement of pan at the top and the other one is with the arrangement of the pan at the bottom. In our project we are using the one which has a pan arrangement at the top and this kind of TGA is called as TA Q50, shown in Figure 11. In this model the pan is at the top with the stem support rod. In this kind of TGA the balance precision is up to 0.01 % and its capacity is 1500 mg.The TGA thermal curve is plotted with weight or weight % versus time or temperature. The curve can be studied from left to right and the graph gives the weight loss of the sample.

The sample can be analyzed by identifying the temperature were the actual weight loss is started and also by identifying the inflection point. Inflection point is the point where the greatest rate of weight loss change can be identified on the curve and simply called as 1^{st} derivative peak temperature. In case of any analysis it is recommended to maintain reproducibility and this is recommended even in case of TGA and the factors that affect the reproducibility are furnace cleanliness, sample preparation, calibration, temperature range, sample atmosphere and there are many other factors but this are considered to be important.Calibration is to be done very frequently and if the sample

that is used has the property of coating the furnace then the instrument should be calibrated every day. The ideal sample weight for the analysis is between 2-50 mg. To obtain reproducibility sample weight should be precise. The temperature scan rate can be between 10-50 ^{o}C per minute based on the type of analysis [35]. Calibration is mandatory when there is a change in temperature range or purge gas rate or purge gas or if the instrument is moved.

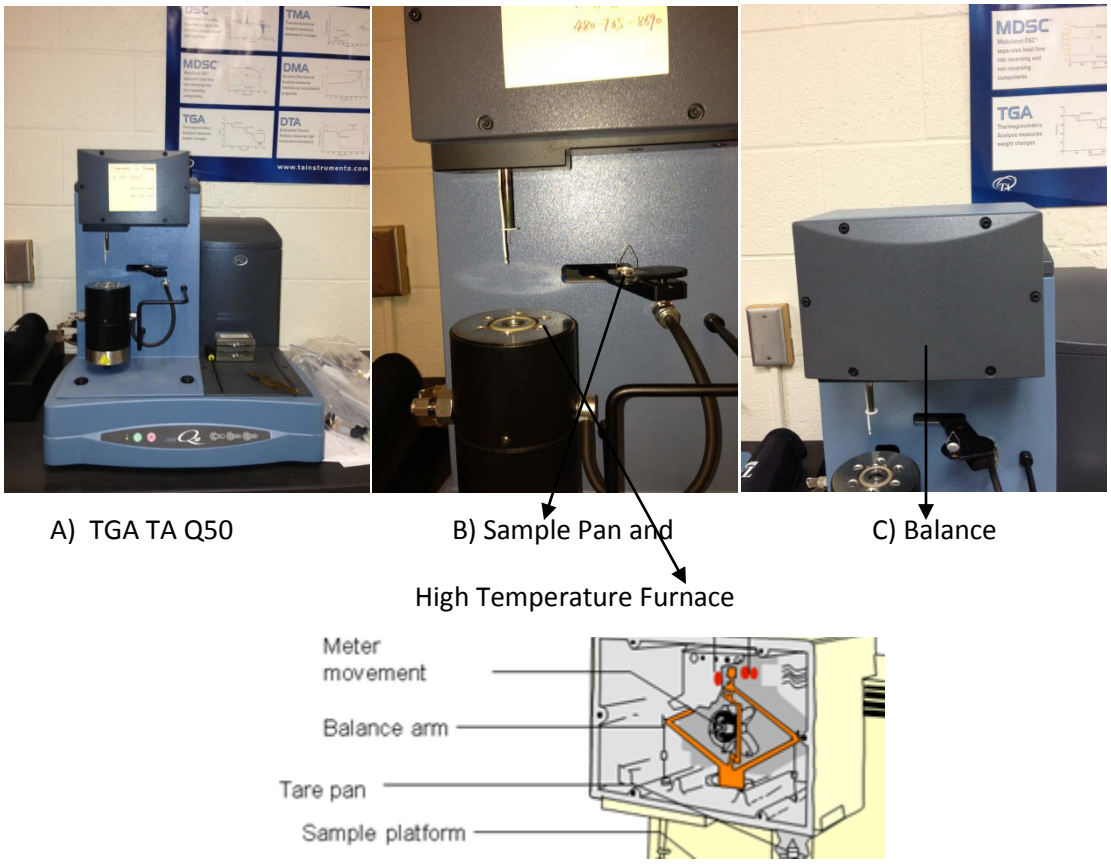

Figure 11: Components TGA TA Q50

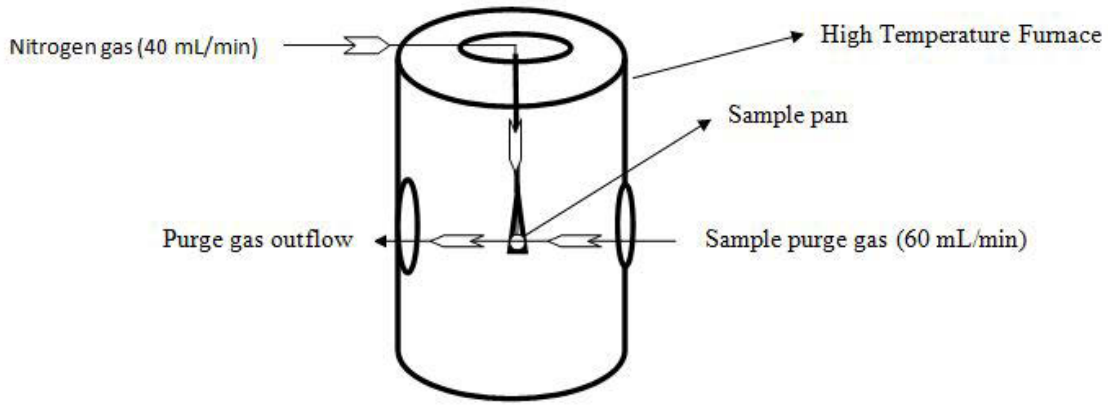

Figure 12: Schematic TGA TA Q50

In our project the model used was TA Q50, shown in Figure 11 and Figure 12. This contains the sample pan at the top. The sample pan used is made up of platinum.The quantity of sample used for the analysis is 5-10 mg. The samples are analyzed in two different atmospheres. One is nitrogen and the other one is 5 % hydrogen in combination with helium. The sample that was run in the hydrogen atmosphere let us know the reduction temperature and the samples that were run in nitrogen atmosphere will give the information regarding the thermal stability and weight loss of the compounds. The samples are heated up to 900^{o}C for the analyses and the heating rate is 10 °C/min. TGA can help in the identification of moisture content by change in weight percentage and also helps in the evaluation of thermal stabilities of the compounds.

2.2.4 Transmission electron microscopy (TEM)

Transmission electron microscope uses beam of electrons as a source instead of light in the light microscope and gives morphologic, crystallographic and compositional information of the specimen. The resolution of TEM is thousand times better than light microscope because of its lower wavelength range of electron (λ_{200kV}=0.00251 nm).

The principle mechanism in TEM involved is the electrons are emitted from the electronsource at the top and that electrons passes through the vacuum and then using the electromagnetic lenses the electrons are focused into a very small electron probethat transmitted through the specimen. Based on the density of the specimen, some of the electrons may disappear from the beam due to the scattering.Theunscattered electrons will display an image of the specimen based on their density which is further can be studied or analyzed. The TEMimages are found to be having very high resolution compared to that of light microscope. The basic components of TEM are electron gun, electromagnetic lenses, vacuum chamber, sample stage, fluorescent screen or other detectors.

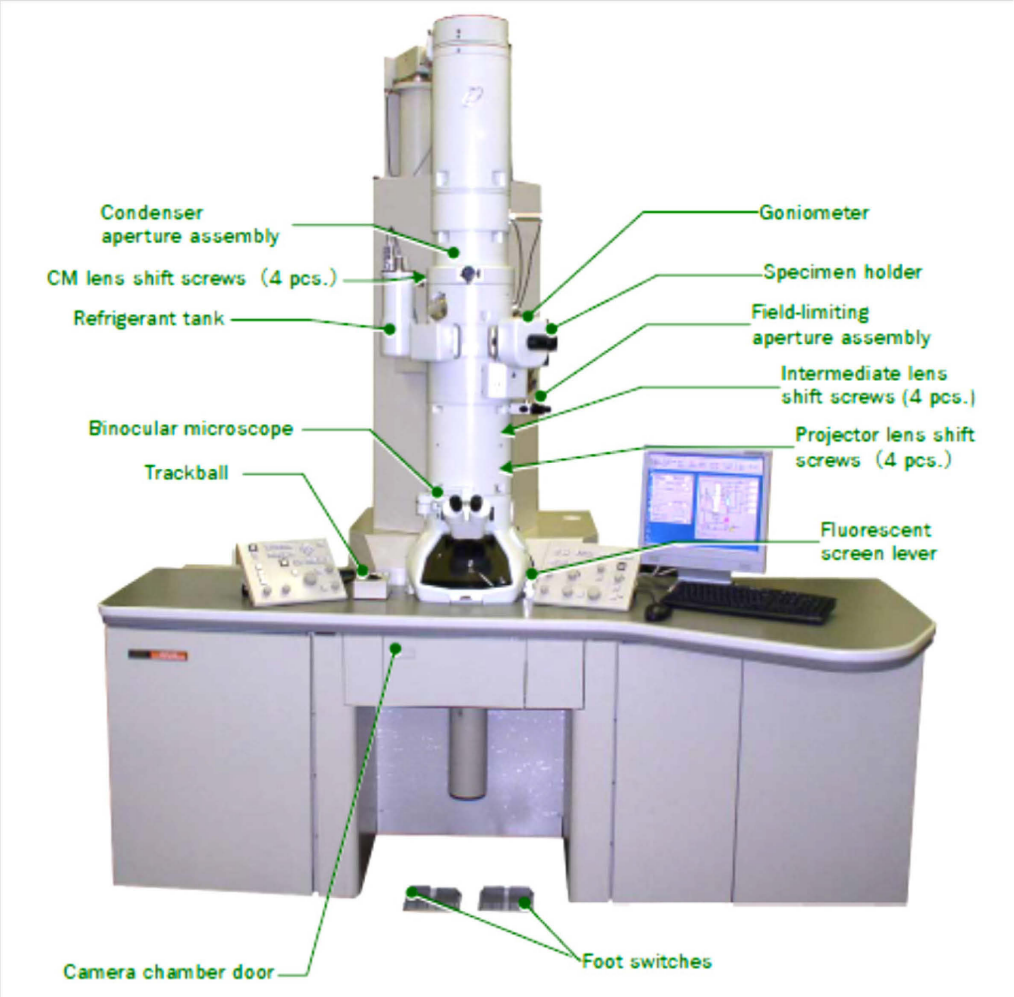

Figure 13: JEOL 2100 Transmission electron microscope (TEM)

For any TEM the lenses are characterized into three stages. The first stage is condenser lenses followed by objective lenses and the projector lenses. Primary beam formation takes place in the condensor lenses and this primary beam is focused through the sample by objective lenses and finally the projector lenses are useful in projecting the beam onto the phosphor screen which is also called as imaging device. The important component in the TEM is vacuum system. The vacuum system is maintained with low pressures on the order of 10^{-4} Pa [36]. The need for this is to maintain mean free path of the electron gas

interaction. The vacuum system needs to be evacuated very frequently to avoid the collision between electrons and gas atoms to negligible levels for a better imaging.

The sample holder also called as specimen holder holds the grids which are standard with a size of 3.05 mm diameter ring having a thickness range of few to 100 μm. The TEM grid materials are made of either copper, molybdenum, gold or platinum. This grid is placed in the sample holder that is paired with the specimen stage. After loading of the sample to the specimen stage the electrons from the electron gun are pumped out on to the anode plate and to the TEM column after connecting the filament to the negative component power supply and final output is displayed on the screen.

In our research the model we used was JEOL 2100, shown in Figure 13. JEOL 2100 has a lanthanum hexaboride (LaB_6) electron source. It has threecondenser lenses (two beam deflector coil condenser lens and one condenser minilens) that helps in acquiring highest probe current for any probe size. JEOL JEM-2100 high resolution scanning/transmission electron microscope (S/TEM) is fitted with an Oxford Instruments INCA energy dispersive X-ray detector (EDX) system with light element detection capability for quantitative analysis. It operates at an acceleration voltage of 200 kV and is equipped with an EDAX Sapphire X-ray energy dispersive system (EDS), bright and dark field detectors for scanning transmission electron microscopy (STEM), two ORIUS digital cameras from Gatan, single and double-tilt holders and an image acquisition and analysis software package (Gatan'sDigitalMicrograph). The instrument can attain a point resolution of 0.194 nm and an information resolution of 0.14 nm. The microscope is used for atomic scale investigation of defects, chemical composition, and crystallographic structure of ceramics, metals, composite nanostructures, semiconductors and

minerals.The combined high resolution/analytical capabilities of the instrument make it particularly suited for characterization of nanometer sized or atomic-level structures. In this study, low magnification TEM images are used to get the information about particle shape and size, while high magnification TEM images offer atomic-level crystallographic structural information.

TEM samples were prepared by using dilute suspensions of the nanopowder samples. These solutions were obtained by ultrasonicating particles in ethanol for 10 min then dropping the suspension of the sample powders onto an ultrathin carbon film/holey carbon, 400 mesh copper grid (from Ted Pella) and letting it air dry for several hours.

In general, TEM helps in analyzing the structure and texture and also used to identify flaws, fractures and damages in micro-sized objects. It also provides topographical, compositional, morphological and crystalline information.

2.2.5 Raman spectroscopy

Raman and Infrared (IR) spectroscopy are categorized under vibrational spectroscopies and these are rather the most common among those categories. Ramanis based on inelastic scattering of monochromatic excitation source. Inelastic scattering can be best defined as the frequency of photons in monochromatic light. That frequency changes when there is an interaction with the sample. The sample will absorb the photons of laser light and they reemit them. The reemitted photons will have varied frequency than compared to that of original and that difference is called as Raman Effect [37]. Information about rotational and vibrational frequencies can be obtained due to these differences. Almost any kind of samples, solid (powders)/liquid/gas, can be analyzed directly.

There are three kinds of frequencies, shown in Figure 14, that are important in case of Raman Effect

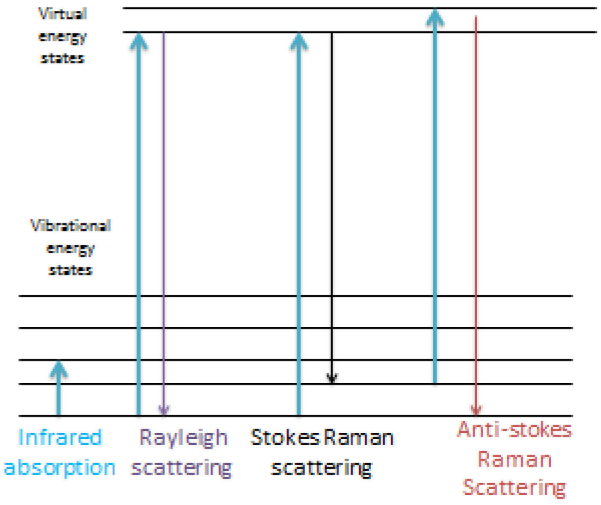

Figure 14: Different frequencies of Raman scattering

The first one is Rayleigh scattering. This is mainly due to absence of active Raman modes in a molecule. Such molecules will absorb the light with a frequency of υ_o(frequency of incident wave)and reemit the light with same frequency.The second one is stokes frequency. This explains that the molecules having Raman active modes will absorb the light with frequency of $\upsilon_o$and reemit the light with a reduced frequency of υ_o-υ_m (stokes Raman frequency)and this frequency is called as stokes frequency and the third one is anti-stokes frequency. In this case the molecules which are already in the excited vibrational state having Raman active modes and this molecules when interacted with light from the laser having a frequency of υ_o, its intensity increases and the scattered light will be with a frequency of $\upsilon_o+\upsilon_m$(Anti-stokes Raman frequency) and this case we call it as anti-stokes frequency.

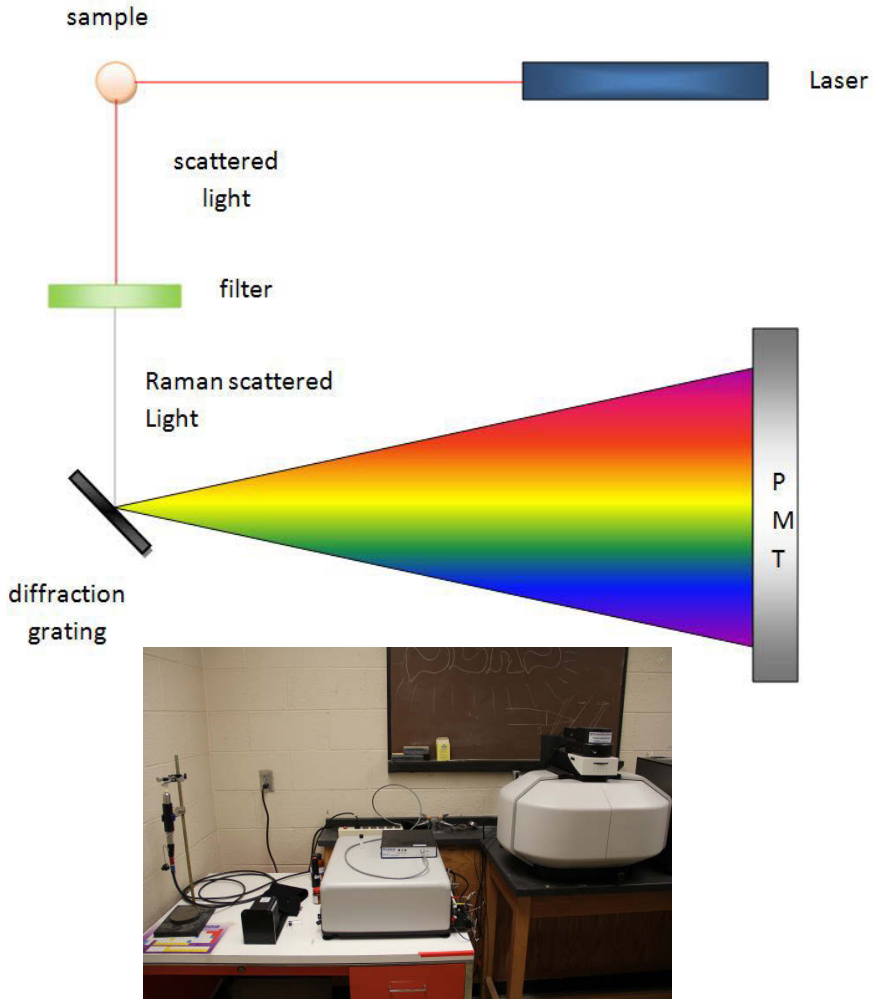

Figure 15: Basic Schematic of Raman spectroscopyand Kaiser RXN1 Raman spectrometer

Raman spectroscopy is mainly intended to determine modes of molecular vibrations. A spectrum is a graphical representation of the light intensity as a function of light frequency. The major light source used is laser. Light from the laser hit the sample which reflect the light and that reflected light will be collected by the detector and the results are displayed. The intensity of the Raman peak is purely depended on the concentration of the active species and it also depends on the polarizability of the molecule, and intensity of the source.

In this project, the Raman spectrometer we used was a Kaiser Optical System (RXN1), shown in Figure 15, consisting of 4 parts: laser, optical lens, wavelength selector and detector. Laser is used as light source and the intensity used for our characterization is 785 nm. The second one is the sample illumination system and light collection optics. The function of this is the sample placed in the sample holder is exposed to the light source. We used the sample holder that is made of quartz. The emitted light from the sample will be collected by a lens and that passes through the interference filter to obtain Raman spectrum.The third one is wave length selector. This includes either filter or spectrophotometer. The light after reflected from the sample passes through this filter or spectrophotometer and then reaches the detector. The fourth and the final one is detector. The commonly used detectors are photodiode array, Charge Coupled Device (CCD) or Photomultiplier tube (PMT). This is the last stage were final data can be analyzed. Nowadays multichannel detectors like PMT or CCD are used. CCD has become the first choice of detectors for Raman spectroscopy. The detector used for our project is PMT detector.

The major problem with the Raman spectroscopy is that the spontaneous Raman scattering is very weak and the other major issue is the intensity of stray light which may exceed the intensity of Raman signal. Many measures were taken to reduce the stray light. In this project, we used 10 second exposure time to get better signal-to-noise ratio. All peak intensities and positions were obtained with Lorentzian fitting. The Raman scattering in the 100-3200cm^{-1} region was collected.

In our study, Raman spectroscopy was employed to analyze the presence of Raman active modes and also to investigate the type of symmetry of cerium oxide,

titanium oxide and $Ce_xTi_{1-x}O_2$ mixed oxides based on their Raman plots. Usually cerium oxide will exhibit a single strong peak which indicates the presence of Raman active mode.

CHAPTER 3: Synthesis and characterization of cerium titanium mixed oxides using precipitation/hydrothermal method

The bulk reduction temperature of the cerium oxide (CeO_2) in general will be very high at around 780-830 ^oC [38]. As stated in Chapter 1 introduction, cerium-based mixed oxides present better low-temperature reducibility and superior thermal stability. In this project, we selected $Ce_xTi_{1-x}O_2$ ($0 \leq x \leq 1$) system and used hydrothermal method to synthesize a series of mixed oxidesnanopowders. A systematic study in synthesizing $Ce_xTi_{1-x}O_2$ ($0 \leq x \leq 1$) with varying compositions was carried out to investigate the composition effect on the reactivity of cerium-based oxides. Using hydrothermal method, the effect of the different parameters (hydrothermal reaction temperature, dwell time, stirring time, and NaOH concentration) was tested on the morphology/size control of pure cerium oxide, titanium oxide, and mixed oxides. This could be able to attain lower temperature reducibility than the present generation compounds. The main goals of our research project were to synthesize the products that are thermally stable, having low temperature reducibility, higher surface area with a better catalytic activity for automotive exhaust gases conversion.

In this study, we employed two different strategies to synthesize $Ce_xTi_{1-x}O_2$ ($0 \leq x \leq 1$) mixed oxides: precipitation/hydrothermal and nanotube template methods. Chapter 3 and Chapter 4 introduce the corresponding results, respectively.

3.1 Synthesisprocedure:

The synthesis procedure remains same for the synthesis of cerium oxide, titanium oxide and$Ce_xTi_{1-x}O_2$mixed oxides. For the synthesis of cerium oxide we used cerium nitrate ($Ce(NO_3)_3$) and for the synthesis of titanium oxide we used titanium chloride ($TiCl_4$) as precursor. For the synthesis of the mixed oxides both cerium nitrate and titanium chloride were used based on the required composition. The concentrations of cerium nitrate and titanium chloride are 0.1 M and the concentration of sodium hydroxide (NaOH) used is 6 M.

Initially 0.1 M titanium chloride, 0.1 M cerium nitrate and 6 M sodium hydroxide were prepared and kept aside as stock solutions and then second step was to mix the cerium nitrate and titanium chloride based on the desiredcomposition for 30 minutes. Then 8 mL of 6 M sodium hydroxide was added and the mixture was stirred continuously for 2 hours at 700 rpm. Once done with mixing the suspension solution was transferred to autoclave for hydrothermal reaction. The hydrothermal reaction was carried in a temperature programmable box furnace using 4-segment system and regarding that it was already explained in Chapter 2. The sample obtained after hydrothermal reaction was further filtered and washed thoroughly using 500 mL of deionized water and 50 mL ethanol. After proper washing with water and ethanol the sample was dried at 50 ^oC for 18 hrs [39-42]. Then the product was extracted from the filter paper and finely grinded for further analysis.

The finally obtained product was used for the sample characterization in a systematic way starting from P-XRD, TPR,BET, TEM and Raman Spectroscopy.

3.2 Characterization:

3.2.1 Cerium oxide (CeO_2):

3.2.1.1: Powder X-ray diffraction (P-XRD):

All the XRD characterization for this study was done on aRigaku Miniflex II diffractometer instrument with a scan speed of 0.5 ^{o}/min in the 2θ range of 5^{o}-90^{o} or 10^{o}-90^{o}equipped with Cu-Kα radiation. As discussed earlier in Chapter 2, XRD is used to study the crystal structure, crystallite size and particle nature based on the diffraction peak patterns.

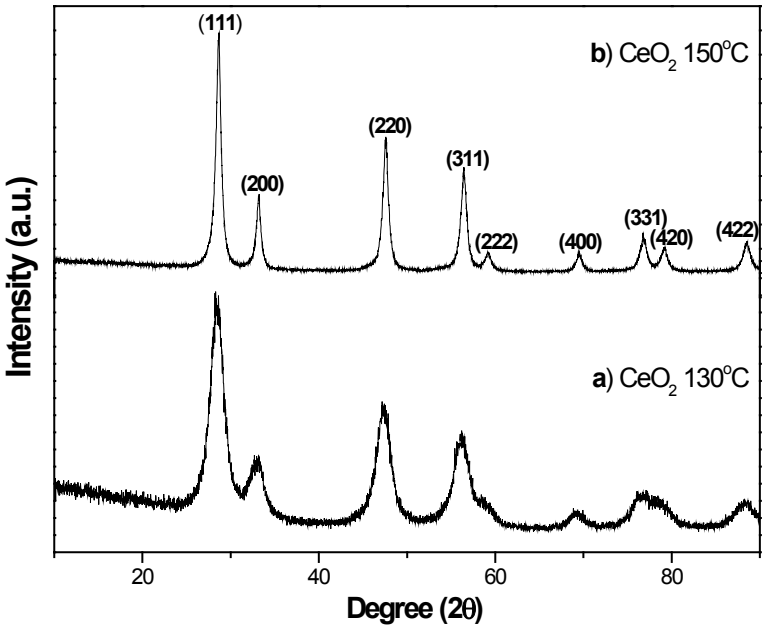

Figure 16: Powder XRD plots of cerium oxidesprepared at different temperatures

Based on the JCPDS card # 34-0394, the structure of as synthesized cerium oxide is face-centeredcubic structure (FCC)or cubic fluorite structure. All the peaks were found to be a perfect match with the JCPDS card data. In our study, we tried to test the effect of hydrothermal reaction temperature on its structure. The synthesis of cerium oxide in two different temperatures revealed that there is a significant effect oncrystalline nature and particle size. Figure 16 shows clearly that with increasing temperature,the cerium oxide gets more crystallized and that effect can be easily seen by the peaks(222) at 59^{o} and

(331) at 78^{o}that became shaper and very well distinguished. The ceria (CeO_2) synthesized at 130 ^{o}C found to have weak and diffused (222) and (331) peaks andare less crystalline than the sample synthesized at 150 ^{o}C. Using (111) peakof cubic CeO_2 average crystallite sizes were estimated by Scherrer equation. The average crystallite size of 130^{o}C samples was 4.5 nm and for 150 ^{o}C samples was 11.1 nm. So, based on the XRD data it can be concluded that with increase in temperature the particle size and crystalline nature of the material also increases.

3.2.1.2: Hydrogen temperature program reduction (H_2-TPR) and BET:

Hydrogen temperature program reduction analyses were conducted on a Micromeritics Autochem 2920 analyzer using U-shaped quartz tube sample holder. About 0.0650-0.0850 g of sample was used for all the analyses with a small amount of glass wool as a loose bed between two glass wool plugs. Samples were analyzed between temperature range of 50-950 ^{o}C at a heating rate of 10 ^{o}C/min and the gas flow used is 5%H_2/95%Ar at a flow rate of 50mL/min. The hydrogen adsorbed ($4CeO_2+H_2 \rightarrow 2Ce_2O_3+H_2O$) will be detected by a TCD (thermal conductivity detector)detector. This is used to analyze the reduction temperature of oxide sample and hydrogen consumption based on the difference in the flow of hydrogen gas on to the detector.

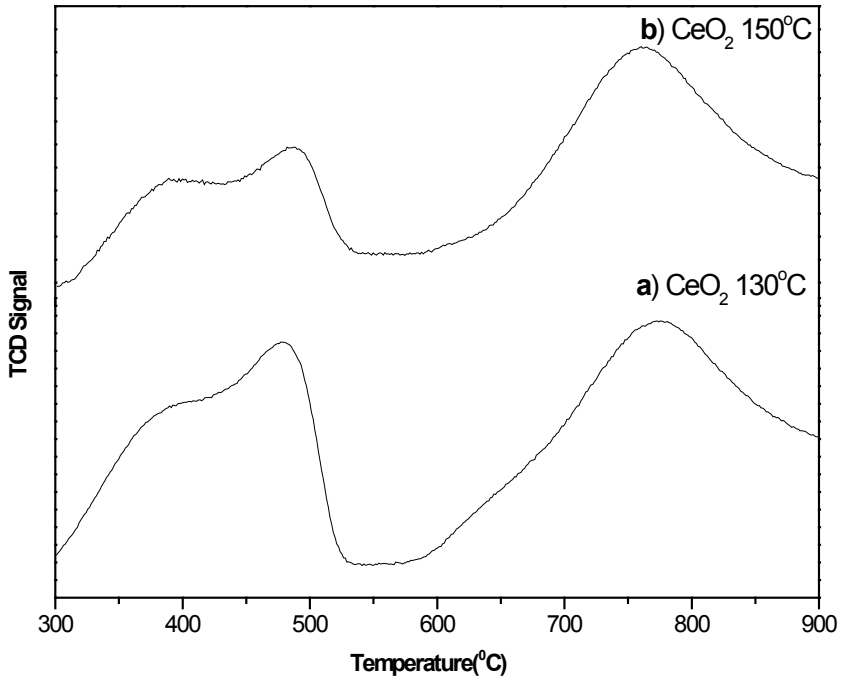

Figure 17: H_2- TPR plots of cerium oxidesprepared at different temperatures

TPR profiles of cerium oxide synthesized at two different temperatures were shown in the Figure 17. Both the samples were found to exhibit almost the same reduction temperatures. Generally ceria will exhibit two kinds of reduction profiles in case of TPR analyses: one is surface reduction and the other one is bulk reduction. The surface reduction temperature for the sample synthesized at 130 ^oC was found to be 481 ^oC and it was 490 ^oC as for 150 ^oC sample. The bulk reduction temperature for 130 ^oC sample was found to be 772 ^oC and for the other sample it was found to be 764 ^oC. This difference in the reduction temperaturecould be due to the slight structural deformation and also might be due to increase in the particle size.

BET measurement:

The Brunauer, Emmett and Teller (BET) surface area analyses were also conducted on Micromeritics 2920 Autochem analyzer. The gas mixture used is Nitrogen in helium and the flow rate is 50 mL/min. The surface area of sample synthesized at 130 ^{o}C has a surface area of 99.55 m^2/g and for the sample at 150 ^{o}C is found to be 49.65 m^2/g. In our study, with increase in temperature the surface area was found to be decreased due to increase in the particle size. The data was found to be in good correlation with the XRD data.

3.2.1.3: Raman spectroscopy:

Raman spectroscopy data was obtained using a Kaiser Optical System (RXN1) having a laser length of 785 nm with a laser exposure time of 10sec for all the samples analyzed.

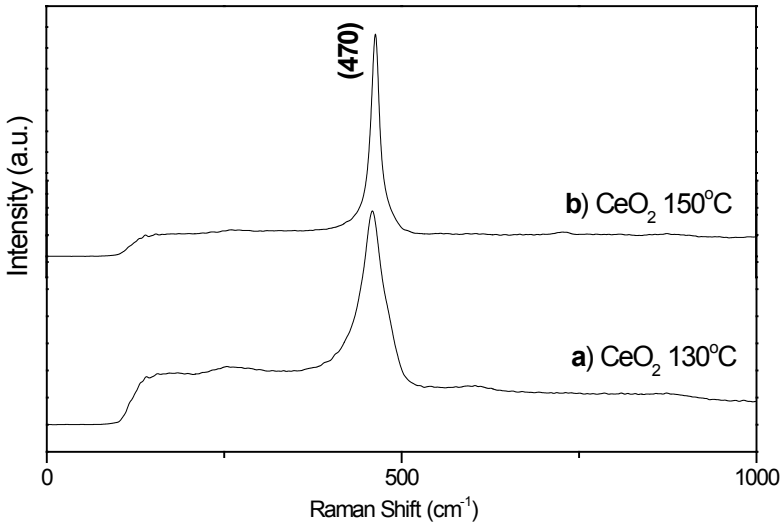

Figure 18: Raman plots of cerium oxides prepared at different temperatures

The data shows a strong intense well defined Raman scattering band. Cerium oxide shows a strong Raman band at 470 cm^{-1}which is similar to many of the previous published results [43]. The strong Raman band is due to its fluorite structure having characteristic Raman active mode [43]. The only major difference between these two samples was there is an oxygen deficient peak at 625 cm^{-1}. Usually the samples synthesized at lower temperature will exhibit some structural defects and due to that reason we are found a The Raman data for the cerium oxide synthesized at two different temperatures did not show much difference in their Raman shift.

3.2.2 Titanium oxide (TiO_2):

3.2.2.1 Powder X- ray diffraction:

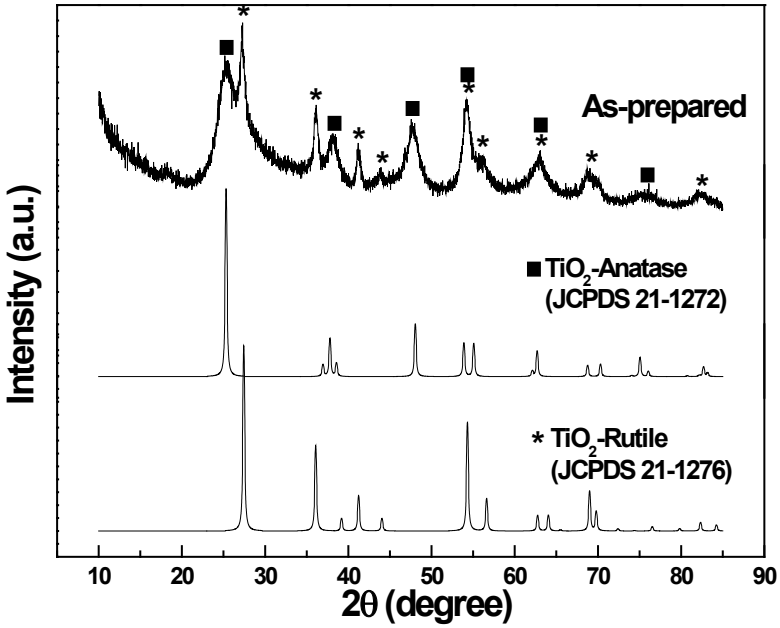

Figure 19: Powder XRD plot of as synthesized titanium oxide in comparison with simulated Anatase and Rutile TiO_2

XRD pattern of as synthesized titanium oxide shows the peak patterns resembling both anatase and rutile phases and it was confirmed using the JCPDS card no. 21-1272 (Anatase) and 21-1276 (Rutile). The XRD pattern of the titanium oxide shown above was synthesized at 150 ^{o}C. Titanium oxide was synthesized at two different temperatures (130 ^{o}C and 150 ^{o}C) and there was no significant difference found based on the XRD. The crystallite size of 150 ^{o}C sample was 10.4 nm and for 130 ^{o}C sample it was 9.9 nm calculated using (111) diffraction peak. With increasing hydrothermal reaction temperature, the super saturation of the suspension solution increased resulting in the increased rate of nucleation and growth and that is the reason for the crystallite size of the materials increased [44].

3.2.2.2 TPR and BET:

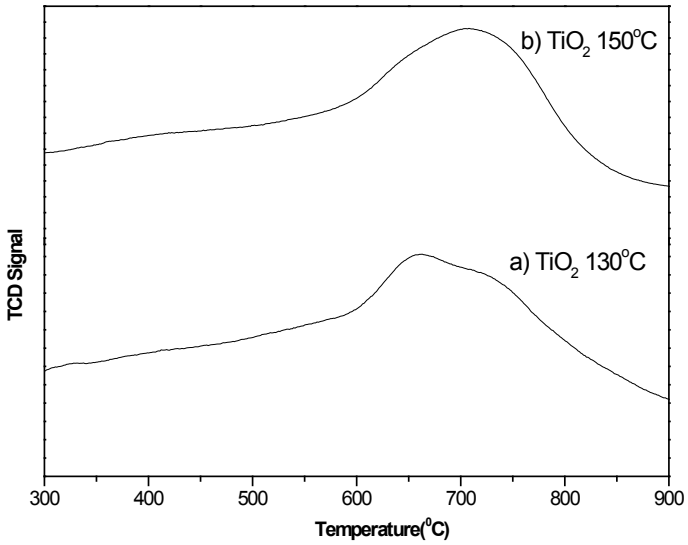

Figure 20: H_2-TPR plots of titanium oxidesprepared at different temperatures

The titanium oxide synthesized at 130 ^{o}C shows a reduction temperature of 666 ^{o}C while the sample synthesized at 150 ^{o}C revealed a reduction temperature of 710 ^{o}C. Titanium oxide prepared at different temperatures has different crystallite size. As

discussed earlier, the crystallite size of the sample increases with increase in temperature. Due to this the reduction temperature also increases with increase in crystallite size.

The BET surface area of both the samples was analyzed using Micromeritics autochem 2920 analyzer. The sample synthesized at 130 ^{o}C was found to have a surface area of 117.21 m^2/g and the sample synthesized at 150 ^{o}C was found to have a surface area of 109.39 m^2/g. These values are in good agreement with the crystallite size calculated using Scherrer equation. Lower crystallite size will yield higher surface area and vice versa. Due to the presence of larger surface area, the titanium oxide synthesized at 130 ^{o}C may exhibit better catalytic activity than the sample synthesized at 150 ^{o}C.

3.2.2.3 Raman spectroscopy:

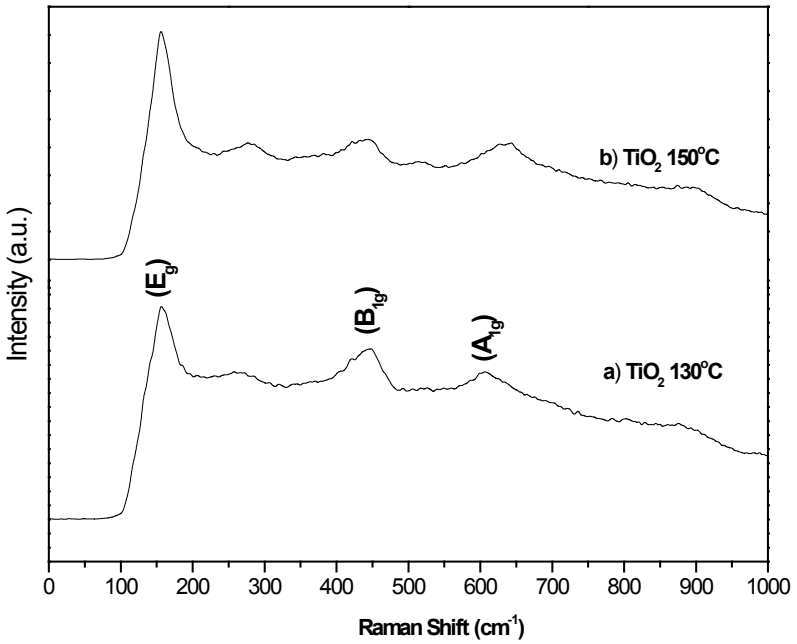

Figure 21: Raman plots of titanium oxides prepared at different temperatures

Raman spectrum for titanium oxide usually will have 3 characteristic Raman scattering bands. As specified in many of the publications,titanium oxide in our study also showed 3 characteristic Raman bands and that include one at 170 cm^{-1}, the second one at 470 cm^{-1} and the third one at 620 cm^{-1} with the symmetries E_g, B_{1g}, and A_{1g}, respectively [45]. There is a slight peak shift observed in all the bands and this indicates that there is slight difference in crystallization in two different samples which was not clearly distinguished in XRD patterns. The strongest peak intensity was absorbed at 170 cm^{-1} and it is of $E_g$symmetry due to the extension vibration of titanium oxide structure.

3.2.3 Mixed Oxide Characterization:

3.2.3.1P-XRD:

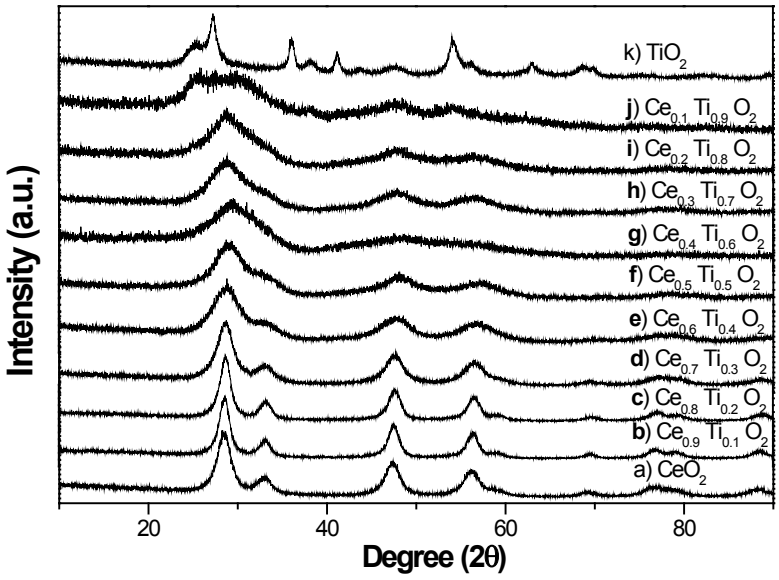

Figure 22: P-XRD plots of cerium titanium mixed oxideswith different compositionsprepared at 130^oC for 48hrs

Figure 22 shows P-XRD patterns of a series of $Ce_xTi_{1-x}O_2(0\leq x\leq 1)$ mixed oxide samples prepared at 130 ^oC using precipitation/hydrothermal method. Cerium oxide was

doped with increasing concentration of titanium oxide starting from 10 % to 90 % to investigate the doping effect of titanium oxide on the structure and reducibility of cerium oxide. As seen in Figure 22, the crystalline nature of the cerium oxide was changed gradually to poorly crystalline with increasing concentrations of titanium oxide from 10 % to 90 %. The doping effect of titanium oxide on ceria can be best studied using the diffraction peaks (111), (220) and (311). Until the doping concentration of titanium oxide was 30 %, the mixed oxide only showed the typical diffraction patterns of cerium oxide without having any traces of titanium oxide. The change in these peaks intensities can be observed when the doping concentration of titanium oxide increased to 40 %. Table 5 gives crystallite sizes of $Ce_xTi_{1-x}O_2$mixed oxides synthesized at 130 ^oC.

Table 5: Crystallite size of $Ce_xTi_{1-x}O_2$ mixed oxides synthesized at 130 ^oC

Composition	Crystallite size(nm)
CeO_2	9.5
$Ce_{0.9}Ti_{0.1}O_2$	5.6
$Ce_{0.8}Ti_{0.2}O_2$	5.4
$Ce_{0.7}Ti_{0.3}O_2$	3.7
$Ce_{0.6}Ti_{0.4}O_2$	2.4
$Ce_{0.5}Ti_{0.5}O_2$	4.4
$Ce_{0.4}Ti_{0.6}O_2$	6.5
$Ce_{0.3}Ti_{0.7}O_2$	7.5
$Ce_{0.2}Ti_{0.8}O_2$	4.6
$Ce_{0.1}Ti_{0.9}O_2$	2.2
TiO_2	9.9

The diffraction peaks (111), (220), (311) became weaker and broader at a concentration of above 50 %Ti-50 %Ce. The crystallite size was also changed moderately

with the increasing concentration of titanium oxide. Initially the crystallite size of the ceria (CeO_2) was high, but it decreased gradually with increase in the doping concentration of titanium oxide. The decrease in the crystallite size of ceria was observed until the doping concentration of titanium oxide reached to 40 %.Then with further increase in the doping concentration until 70 % resulted in increase of crystallite size. Further increase in titanium oxide concentration resulted in decrease of crystallite size. Crystallite size for each composition were calculated and shown in the table3.

Figure 22 gives a clear idea of transformation of crystalline nature into poorly crystalline or amorphous nature. Addition of 10% titanium oxide resulted in the drastic change of crystallite size from 9.5nm to 5.6nm. The average crystallite size of each mixture was calculated using the (111) peak at 29^o assuming a cubic structure.The peak at 29^o was found to be the perfect fit in all the cases. The percentage crystallinity decreased with an increase in doping concentration of titanium into cerium oxide [46]. This decrease in crystallinity and crystallite size from $Ce_{0.9}Ti_{0.1}O_2$till $Ce_{0.1}Ti_{0.9}O_2$is mainly because of phase change/structural transformation from cubic fluorite structure to tetragonal structure.

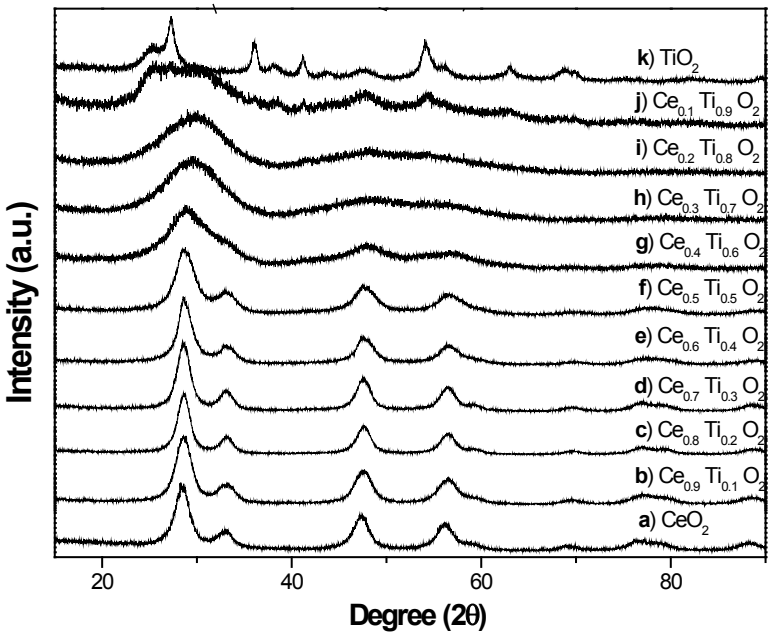

Figure 23: P-XRD plots of cerium titanium mixed oxides with different compositionsprepared at 150^{o}C for 48hrs

The P-XRD diffraction pattern for the samples synthesized at 130^{o}C and 150^{o}C is found to be similar. In both the casesthe typical diffraction peaks(111), (220) and (31 1)gradually became weaker and broader after the concentration of titanium oxide exceeded above60 %.Table 6gives crystallite sizes of $Ce_xTi_{1-x}O_2$mixed oxides synthesized at 150 ^{o}C.

As explained earlier, the crystallite size of pure compounds (CeO_2or TiO_2) will always be higher than the doped compounds. This hypothesis was proved in our study. The compounds synthesized at 130^{o}C and 150 ^{o}C followed the same trend as specified by other researches. The crystallite size of pure cerium oxide was calculated as 6.3 nm which is obtained using the (111) peak at 29^{o} and after the addition of 10 % Ti it was decreased to 4.2nm.The crystallite size of titanium oxide was calculated as 10.4nm. Doping of titanium oxide with 10 % cerium oxide resulted in decrease of its crystallite size drastically to 3.9 nm.

Table 6: Crystallite size of $Ce_xTi_{1-x}O_2$ mixed oxides synthesized at 150^oC

Composition	Crystallite size(nm)
CeO_2	6.3
$Ce_{0.9}Ti_{0.1}O_2$	4.2
$Ce_{0.8}Ti_{0.2}O_2$	2.7
$Ce_{0.7}Ti_{0.3}O_2$	5.1
$Ce_{0.6}Ti_{0.4}O_2$	5.1
$Ce_{0.5}Ti_{0.5}O_2$	5.1
$Ce_{0.4}Ti_{0.6}O_2$	5.5
$Ce_{0.3}Ti_{0.7}O_2$	2.7
$Ce_{0.2}Ti_{0.8}O_2$	2.6
$Ce_{0.1}Ti_{0.9}O_2$	3.9
TiO_2	10.4

Increase in doping concentration of cerium oxide to 20 % resulted in further decrease of crystallite size to 2.6 nm. Usually crystallite size decreases with increase in doping concentration to a certain threshold level. If the concentration exceeds that threshold level then it will result in increase of crystallite size instead of decreasing and this happens due to structural transformation from one phase to other.

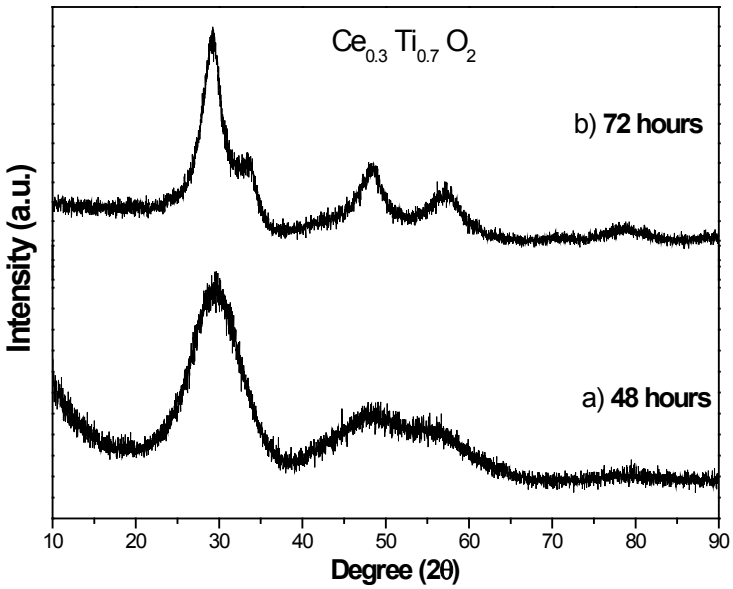

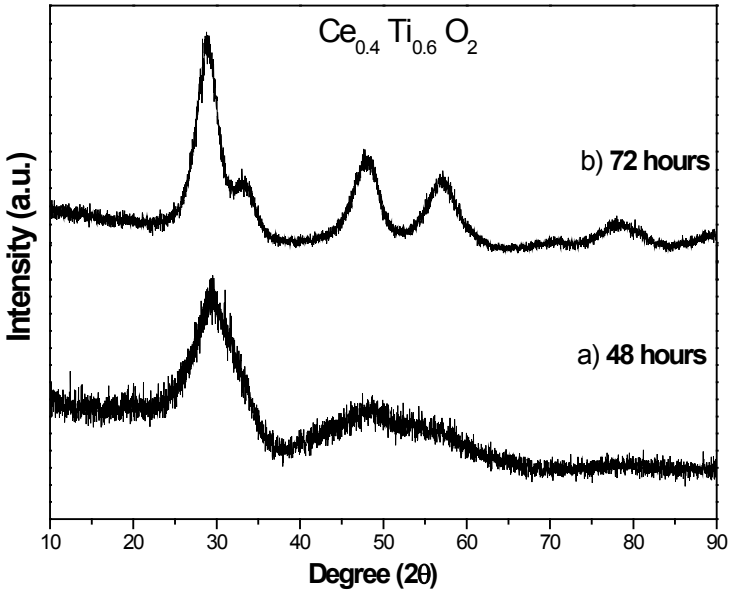

Figure 24: P-XRD plots of $Ce_{0.4}Ti_{0.6}O_2$prepared at 150 ^{o}Cwith different dwell time

As discussed earlier, effects of different experimental parameters on the mixed oxides synthesis were investigated. First of all, the effect of dwell time was studied. The major effect reported due to increased dwell time was an increase in crystallinity

determined based on P-XRD data shown in figure 24 [41]. It was found that the average crystallite size for the $Ce_{0.4}Ti_{0.6}O_2$sample synthesized with a dwell time of 72hrs is 6.5 nm and for the $Ce_{0.3}Ti_{0.7}O_2$sample it is 3.4nm. With a dwell time of 48 hrs, the $Ce_{0.4}Ti_{0.6}O_2$sample the crystallite size is 5.5nm and for the $Ce_{0.3}Ti_{0.7}O_2$sampleit is 2.7nm. Thus, the average crystallite size of the samples synthesized using 72 hrs dwell time is larger than that of the 48 hrs sample and the 72 hrs sample also shows better crystallinity based on XRD and TEM analysis. Generally speaking, if the sample exhibits lower crystallite size then it will be having higher surface area, which is essential for higher catalytic activity.

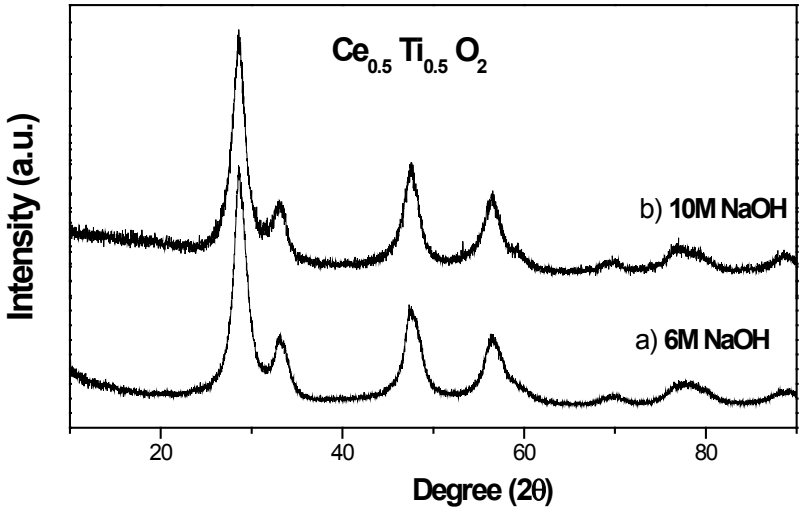

Figure 25: P-XRD plots of $Ce_{0.5}Ti_{0.5}O_2$prepared at 150 ^oC with different NaOH concentrations

Secondly, theconcentration effect of NaOH on the formation of cerium titanium mixed oxide was studied shown in Figure 25; it was found that there is not much difference found in the P-XRD patterns with the change in the concentration of sodium hydroxide from 6 M to 10 M. The reason could bebecause of using relatively small amount of sodium hydroxide (8 mL NaOH and 88 mL mixture of cerium and titanium

precursor). It should be pointed out that there is a significant effect on the formation of mixed oxide if large amount of NaOH is usedwhich is discussed later on in Chapter 4. The crystallite size for the sample synthesized with a concentration of 6M NaOH is 5.1 nm and for the sample synthesized using10 M NaOH is 4.9 nm. The crystallite size of two different samples was calculated and it does not show much difference indicating that change in concentration of sodium hydroxide does not affect the mixed oxide synthesis.

Usually sodium hydroxide with higher concentration will have a significant effect on the synthesis of cerium titanium mixed oxide [39]. But this effect can be seen only when sodium hydroxide is used as a solvent instead of just precipitant [40]. Compounds that are synthesized using sodium hydroxide as solvent will exhibit far better crystallinity than the compounds synthesized using sodium hydroxide in small amounts. The effect of NaOH is further discussed in the Chapter 4. Many earlier researches were conducted to synthesize cerium-based mixed oxides only by using 6 M sodium hydroxide [30].

So, based on the XRD data it can be concluded that increase of NaOH concentration from 6 M to 10 M does not affect the nucleation and growth of $Ce_{0.5}Ti_{0.5}O_2$.

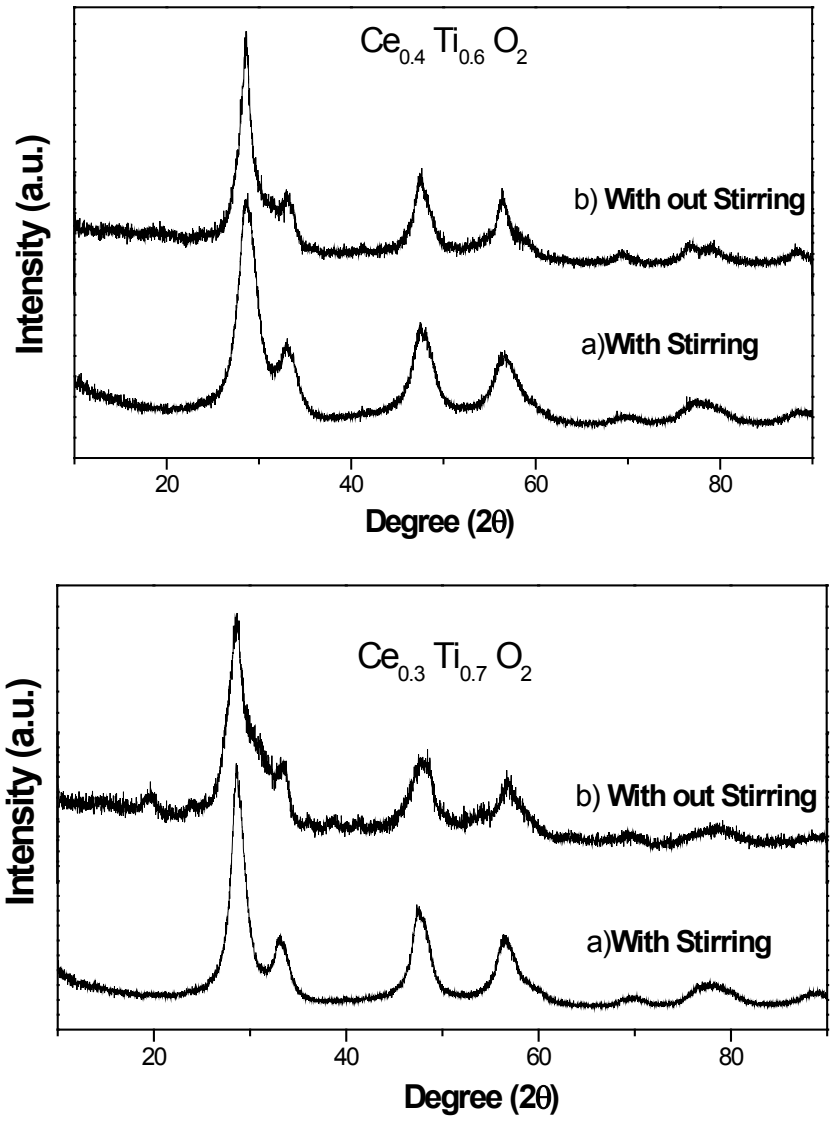

Figure 26: P-XRD plots of cerium titanium mixed oxides ($Ce_{0.3}Ti_{0.7}O_2$ and $Ce_{0.4}Ti_{0.6}O_2$) showing the stirring effect on the compositional homogeneity of mixed oxides

Then the stirring effect on the formation of cerium titanium mixed oxide was investigated, as shown in Figure 26. The average crystallite size was calculated for both the samples. For the sample $Ce_{0.4}Ti_{0.6}O_2$it was 3.9nm and for the sample $Ce_{0.3}Ti_{0.7}O_2$it was 2.5nm. Based on the P-XRD data it can be concluded that mixed oxide synthesized without stirring exhibit poor crystallinity. This poor crystallinity may be due to improper

dissolution of titanium oxide into cerium oxide lattice. So, it is not possible to attain highly crystalline compounds without stirring.

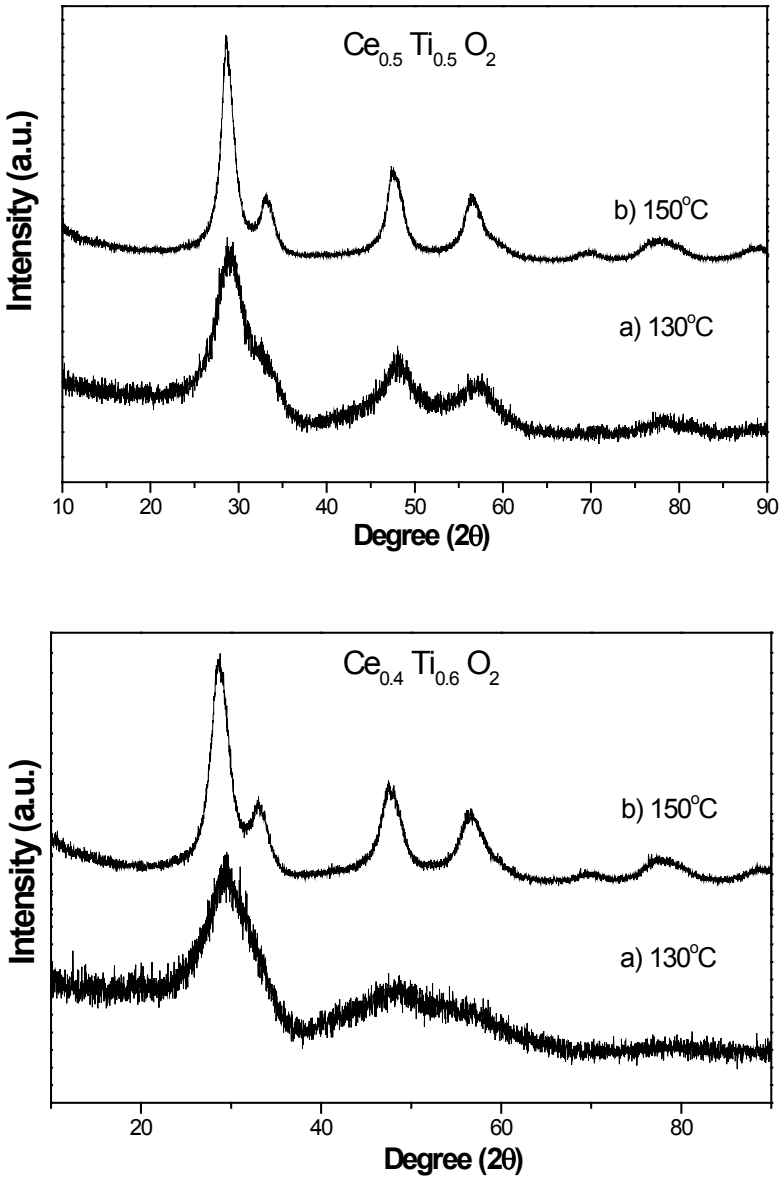

Figure 27: P-XRD plots of cerium titanium mixed oxides ($Ce_{0.5}Ti_{0.5}O_2$ and $Ce_{0.4}Ti_{0.6}O_2$) showing the temperature effect on the crystallinity of mixed oxides

Temperature effect was investigated on two different compositions of mixed oxide. It is very obvious that the sample synthesized at 150 ^{o}C will exhibit higher crystallinity than the sample synthesized at 130 ^{o}C. Generally, at higher temperatures the

atoms in the metal oxides will be arranged in an order. This orderly arrangement of atoms at higher temperature may be the reason for better crystallinity. Theaverage crystallite size for the sample $Ce_{0.5}Ti_{0.5}O_2$synthesized at 130$^oC$was 4.4 nm and the sample synthesized at 150 ^oC was 5.1 nm.

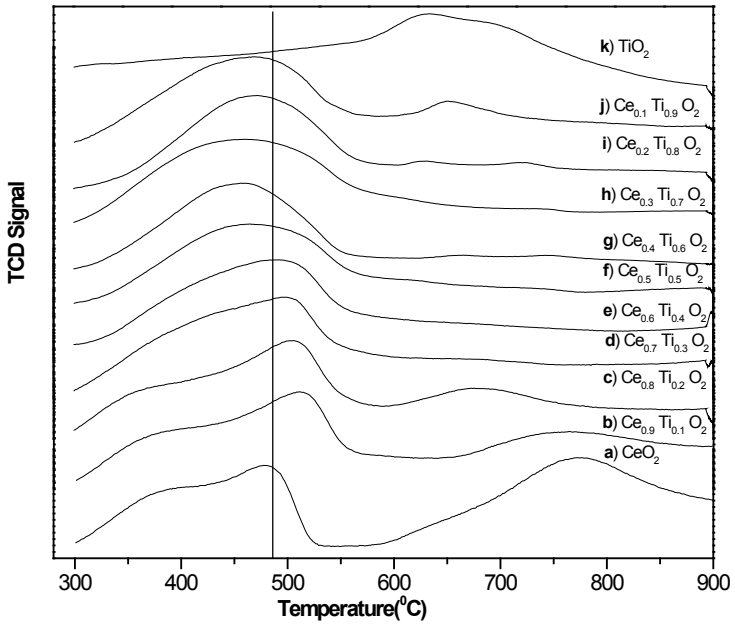

Figure 28: H_2-TPR plots of cerium titanium mixed oxide at different compositions prepared at 130 ^oC using precipitation/hydrothermal method

3.2.3.2 H_2-TPR:

Different samples were synthesized with increased doping concentration of titanium oxide into cerium oxide. Due to its varied crystallite size and lattice parameters the samples tend to exhibit different kinds of reduction temperatures. As synthesized cerium oxide in its pure phase found to have a surface reduction temperature at 479 ^oC and the bulk reduction temperature is 778 ^oC. With increasing concentration of titanium oxide mixing with cerium oxide the reduction temperature found to decrease drastically.

The reduction temperature patterns are shown in the Table 7. All alone ceria or titanium oxide cannot exhibit lower reduction temperatures.

Table 7: Reduction temperature and surface area of $Ce_xTi_{1-x}O_2$ mixed oxides synthesized 130 ^oC

Sample composition	BET surface area (m^2/g)	Reduction temperature(^oC)
CeO_2	**99.55**	479/778
$Ce_{0.9}Ti_{0.1}O_2$	89.08	523
$Ce_{0.8}Ti_{0.2}O_2$	92.03	514
$Ce_{0.7}Ti_{0.3}O_2$	107.87	511
$Ce_{0.6}Ti_{0.4}O_2$	116.06	508
$Ce_{0.5}Ti_{0.5}O_2$	108.49	485
$Ce_{0.4}Ti_{0.6}O_2$	112.91	476
$Ce_{0.3}Ti_{0.7}O_2$	61.11	466
$Ce_{0.2}Ti_{0.8}O_2$	120.97	485
$Ce_{0.1}Ti_{0.9}O_2$	134.13	485
TiO_2	117.21	663

In case of pure ceria/titanium oxide the movement of the oxygen ion in the crystal will not be free and it will take a lot of effort to get the oxygen out of the crystal. This is one of the reasonsfor its higher reduction temperatures. But when ceria is mixed with titanium oxide the oxygen ion moves freely in the crystal, exchanges rapidly with the hydrogen gas and forms water molecule. This free movement of oxygen ions from internal part to the surfaceresulted in the smaller reduction temperatures. Increase in the

doping concentration of titanium till 70 % yielded lower reduction temperatures but with further increase in the doping concentration resulted in higher reduction temperatures. This effect may be due to increase in the lattice parameter and structural change from cubic phase to tetragonal phase. Even in the XRD it was shown clearly that at 80 % Ti, major part of the peaks corresponded to titanium oxide. So, it can be concluded that reduction temperatures can be lowered by doping the titanium oxide only to a certain extent. Doping more than the limit resulted in an increase in the reduction temperature.

BET:

The surface area of cerium oxide, titanium oxide and cerium titanium mixed oxide samples were analyzed using Micromeritics 2920 autochem analyzer and different samples tend to exhibit different surface areas. The surface area of cerium oxide and titanium oxide were 99.55 and 117.21 m^2/g respectively. In general the surface areas of the commercial pure ceria/titanium oxide will be very less compared to that of the as synthesized samples. The surface area of the cerium oxide increases gradually with increase in the doping concentration of titanium oxide. Generally increase in surface area with increase in the dopant concentration was due to inhibition of individual crystallization during precipitation. Due to this the particles exhibited smaller crystallite sizes in nanometers range which was already shown using XRD plots. The highest surface area was 134.13 m^2/g which was shown by sample $Ce_{0.1}Ti_{0.9}O_2$and next was 120.97 m^2/g and that is by $Ce_{0.2}Ti_{0.8}O_2$. The mixing of titanium oxide to cerium oxide is the main reason for acquiring high surface areas for these mixed oxides.

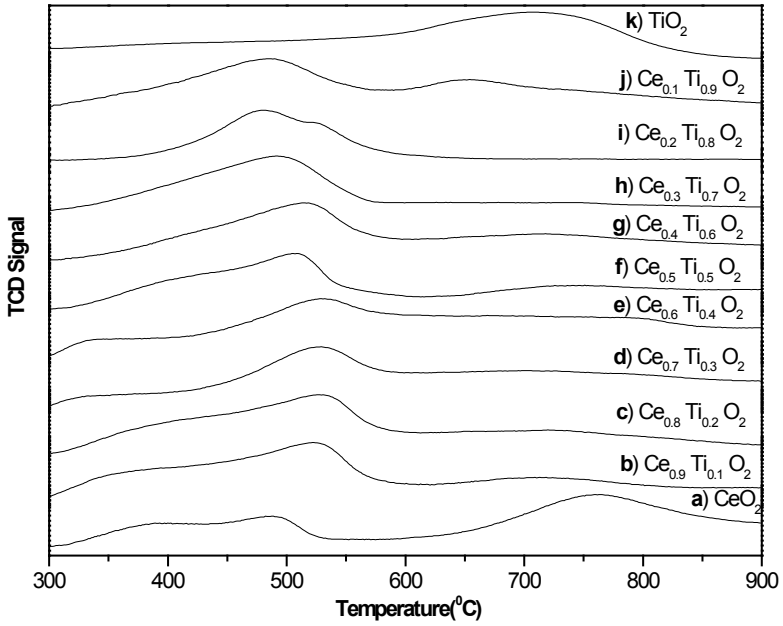

Figure 29: H_2-TPR plots of cerium titanium mixed oxide of different compositions synthesized at 150 ^oC

The samples synthesized with different temperature range to determine its effect on the formation of mixed oxide solid solution. It was found that there is a significant effect on the surface area but not much effect on reduction temperature. The samples synthesized at 130 ^oC also has similar reduction temperature has compared to that of samples synthesized at 150 ^oC. The surface reduction temperature of as synthesized cerium oxide was 483 ^oC and the bulk reduction temperature is 783.3 ^oC. It was almost same as 130 ^oC samples. Other mixed oxides solid solutions were also exhibiting the same kind of reduction patterns. Generally with increase in temperature the particle size also increases which results in the free movement of oxygen ions within the crystal and helps in lowering of reduction temperatures. But in our study, there is not much difference observed in the reduction temperature because of smaller difference between the two temperatures (130 ^oC and 150 ^oC) used for synthesis. The reduction temperatures of various samples were shown in the Table 8 below.

Table 8: Reduction temperature and surface area of $Ce_xTi_{1-x}O_2$ mixed oxides synthesized at 150 ^oC

Sample composition	BET surface area (m^2/g)	Reduction temperature(^oC)
CeO_2	84.0	483.0/783.3
$Ce_{0.9}Ti_{0.1}O_2$	119.3	526.4
$Ce_{0.8}Ti_{0.2}O_2$	97.1	516.8
$Ce_{0.7}Ti_{0.3}O_2$	97.9	510.2
$Ce_{0.6}Ti_{0.4}O_2$	94.4	532.4
$Ce_{0.5}Ti_{0.5}O_2$	96.1	540.3
$Ce_{0.4}Ti_{0.6}O_2$	116.5	532.1
$Ce_{0.3}Ti_{0.7}O_2$	126.9	481.2
$Ce_{0.2}Ti_{0.8}O_2$	145.6	494.7
$Ce_{0.1}Ti_{0.9}O_2$	150.9	485.2
TiO_2	109.39	717.6

BET:

The BET surface area of pure ceria and titanium oxide synthesized at 150 ^oC was 84 m^2/g and 109.39 m^2/g respectively. The surface area of these two samples was found to be lower compared to that of the samples synthesized at 130 ^oC. As discussed earlier there is not much difference noticed because of smaller difference in temperature used for synthesis. The highest surface was 150.9 m^2/g which was shown by the sample having 90 % titanium followed by 145.6 m^2/g shown by the sample having 80 % titanium. But due

to lower crystallization and lower crystallite size the samples synthesized at 150 ^{o}C exhibited better surface areas than the samples synthesized at 130 ^{o}C.

3.2.3.3 TEM:

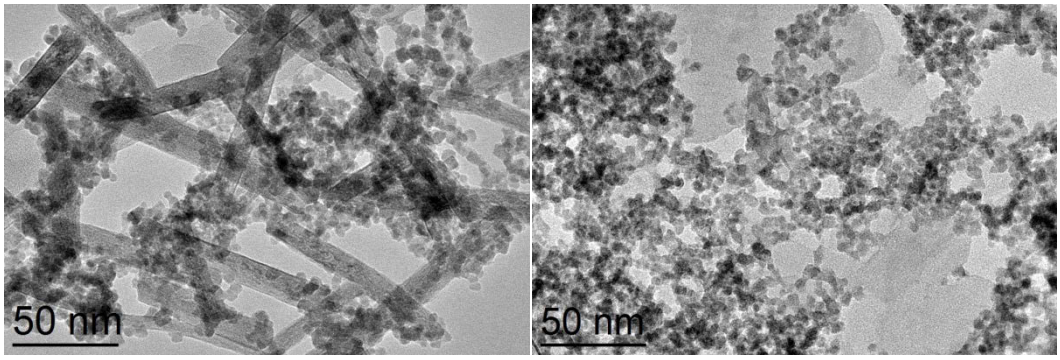

Figure 30: TEM image of (a) $Ce_{0.7}Ti_{0.3}O_2$(b) $Ce_{0.3}Ti_{0.7}O_2$

The TEM images shown in Figure 30 illustrate the presence of both titanium oxide nanotubes and the cerium oxide crystallites. Even in the XRD data it was found that at this concentration the peaks correspondto cerium oxide and that indicates the titanium oxide was not completely substituted into the cerium lattice and hence this mixed phase can be observed clearly in the TEM image. The crystallite size of these particles was found to be 3.7nm with a surface area of 107.87m^2/g. Although there aresome of the titanium oxide nanotubes found but the particle size was calculated for cerium crystallites as the major portion was shared by cerium oxide crystallites. The crystallite size was calculated based on the XRD data. The surface area was obtained from the BET surface area analysis [47-50].

The TEM image of $Ce_{0.3}Ti_{0.7}O_2$composition shows a clear contrast from the TEM image of $Ce_{0.7}Ti_{0.3}O_2$. The particles shown in the image are uniform and also don't show any titanium oxide nanotube structures. This image gives a clear idea that titanium oxide

was substituted into the cerium lattice and it also supports the XRD data. The crystallite size was 2.7 nm was calculated based on the XRD data and the surface area was 126.9 m^2/g obtained from BET surface area.

3.2.3.4 Raman spectroscopy:

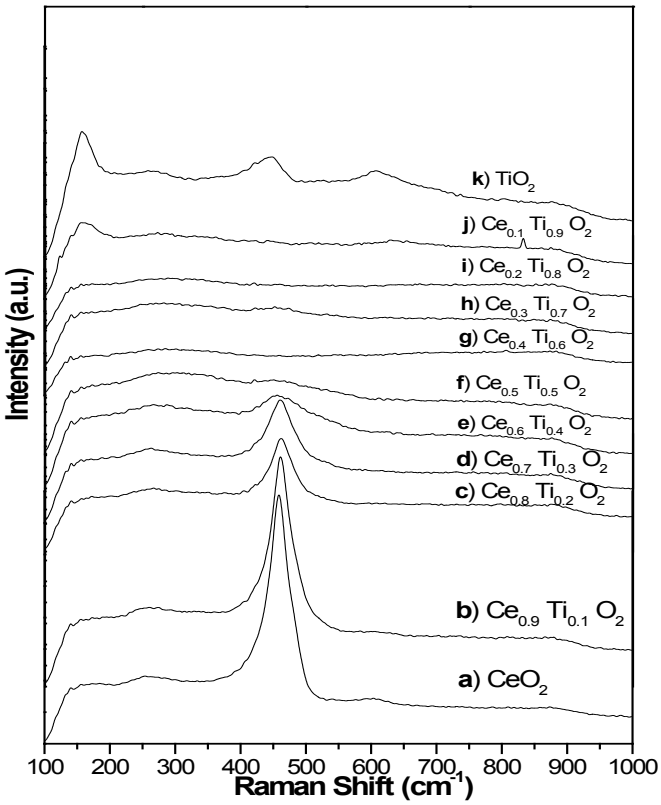

Figure 31: Raman spectra of cerium titanium mixed oxides with different compositions prepared at 130 ^oC using hydrothermal reaction

Raman spectroscopy of different mixed oxide solid solution samples were analyzed and found very characteristic Raman bands. The cerium oxide synthesized in the lab showed an intense Raman band at 460 cm^{-1} and after mixing 10 % titanium oxide there was a slight shift in the Raman band and the intensity is reduced. At a concentration of 30 % titanium oxide the peak intensity reduced a lot and with further increase in the titanium concentration resulted in complete dissolution of the peak. With increased

concentration of the titanium oxide resulted in peak shift towards pure titanium oxide. The peak patterns reveal that the solution is mixed oxide solid solution with no other extra Raman bands.

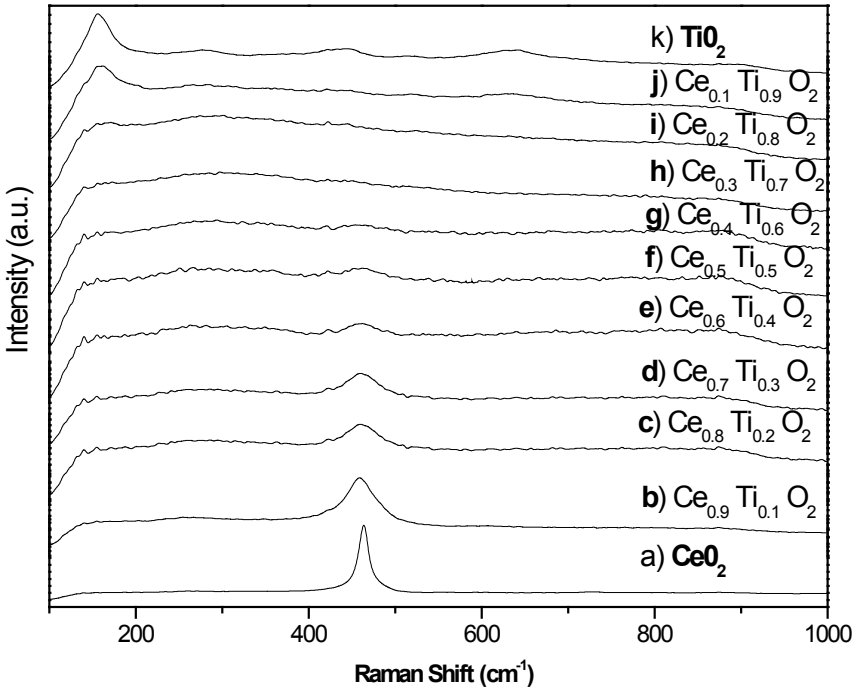

Figure 32: Raman spectra of cerium titanium mixed oxides with different compositions prepared at 150 ^{o}C using hydrothermal reaction

Even for the samples synthesized at 150 ^{o}C it followed the same kind of peak patterns. The peak found to shift towards titanium oxide when the mixing concentration of titanium oxide reached to 40 %. All peaks were found to be in match with the samples synthesized at 130 ^{o}C except some samples which tend to show slight peak shift but not that characteristic. From top to bottom that is with increasing concentration of cerium oxide it was found that there is a blue shift of Raman active bands towards higher wave number.

3.3 Conclusion:

The synthesis of cerium oxide, titanium oxide and cerium titanium mixed oxides was done using precipitation/hydrothermal method. As stated earlier the main goals of the project were to synthesize nanomaterials with better thermal stability, higher surface area and lower temperature reducibility. Materials with higher surface area (126.9 m^2/g) and better temperature reducibility (466 ^oC) were synthesized.

The only major problem with the precipitation method was we are unable to synthesize shape-controlled and thermally stable compounds. Nanomaterials tend to have more thermal stability and better activity than the mixed oxides. In particular it was stated by many researchers that the nanomaterials having alkaline nature will exhibit better thermal stability than regular nanomaterials. So, we have decided to synthesize nanomaterials having a sodium element substituted into their lattice.

We made some slight modifications to this precipitation procedure in order to overcome these problems. This lead to the use of nanotube template method to overcome this problems and this can be discussed in the later chapter.

CHAPTER 4: Synthesis and characterization of$Ce_xTi_{1-x}O_2$ nanostructures using nanotube template method

As we discussed earlier in Chapter 1, cerium oxide has been used as an additive in the automotive three way catalyst since a long time, but because of its drawbacks (such as undergoing sintering under high temperatures, higher reduction temperature, lower low-temperature catalytic activity) researchers developedcerium-based mixed oxides doped with other rare earth metal oxides (PrO_2, TbO_2), the group IVB metal oxides (ZrO_2, TiO_2, HfO_2), and some transition metal oxides (Co_3O_4, NiO, CuO) which can yield better results. Among these cerium-based mixed oxides, the doping of titanium oxide in ceria seemsthat givesbetter results than other oxides and the results were shown in table 2 in Chapter 1.

The mechanism by which the addition of other oxides enhances the low-temperature properties is not yet well understood, but it likely involves the creation and stabilization of oxygen vacancies in the ceria lattice [18].It has been reported that the addition of titanium oxide in ceriacan enhance the cerium oxide activity by changing its electronic properties and by changing its lattice structure. Titanium oxide can easily switch between the Ti^{+3} andTi^{+4} which is a major advantage, due to that the enhanced catalytic activity was exhibited when mixed with cerium oxide. Titanium oxide (0.064 nm) because of its ionic radiusit is easy to introduce into the ceria (0.097 nm) lattice and that will result in enhanced catalytic properties.

4.1 Synthesis procedure:

The synthesis procedure using nanotube-template method was different for each of titanium oxide, cerium oxide and also for cerium titanium mixed oxide nanotubes.

4.1.1 Synthesis of titanium oxide:

Firstly 2 g of titanium oxide powder was added to 80 mL of 10M NaOH and thenthe suspensionwas mixed and stirred for 24hrs. The stirred solution was transferred to a 200mL autoclave. Further, the hydrothermal reaction was continued in a programmable box furnace. The temperature for the reaction was 150^{o}C and the dwell time used was 72hrs. The total number of segments that we used for the synthesis was four and each segment has its own criteria and the functions of each segment were explained in the Chapter 2.

The sample that was obtained was filtered first with 40 mL of 0.1M HCl and then with 500 mL of water,and the final product was dried in an oven at 80^{o}C for 24 hrs. Before drying the powder, a TEM sample was prepared in order to get well-dispersed nanostructures.

For the synthesis of titanium oxide nanotube, the experimental procedure was changed slightly. In general, the synthesis procedure of titanium oxide and cerium oxide were same but the only major change was the dried product was calcined at 400, 500, 600^{o}C for 2hrs. The reason behind this change is due to that the initial synthesized product was hydrogen titanate. In order to prepare titanium oxide, a further thermal treatment is necessary to decompose hydrogen titanate to titanium oxide [39-40].

4.1.2Synthesis of cerium oxide:

Usually the synthesis procedure of titanium oxide and cerium oxide were same except calcination step. 2 g of cerium nitrate was weighed and mixed with 80 mL of 10 M sodium hydroxide and stirred it for 24 hrs and then the suspension was transferred to programmable box furnace for hydrothermal synthesis using a dwell time of 72 hrs. Then after 72 hrs the obtained precipitate was washed using 40 mL of diluted HCl and 500 mL of water. Then the product was dried at 80 ^{o}C for 24 hrs.

4.1.3 Synthesis of mixed oxide nanostructures:

Firstly the precursors were prepared: 0.1M titanium oxide suspension solution, 0.1M cerium nitrate solution, and 10M sodium hydroxide were prepared.

Based on the percentage composition required ($Ce_xTi_{1-x}O_2$, x=0.1, 0.2, 0.3, 0.4, 0.5, 0.6), for example, to prepare 70 % titanium and 30 % cerium oxide ($Ce_{0.3}Ti_{0.7}O_2$), 3.5 mL of 0.1 M titanium oxide and 1.5 mL of 0.1 M cerium nitrate were mixed (5 mL total).Then the mixture was stirred for 2 hrs. Following that, 80 mL of 10M NaOH is added to the mixed solution [41-43]. Another 24 hrs stirring was applied to the suspension. Then the stirred suspensionwas transferred to a 200 mL autoclave and the temperature used for the hydrothermal reaction was 150^{o}C. The dwell time used was 72 hrs. The same four segment system was followed for the experiment. The products obtained were characterized as mentioned earlier usingP-XRD, BET, H_2-TPR, TEM and Raman spectroscopy.

Table 9: Comparison between precipitation/hydrothermal method (Chapter 3) and nanotube template method (Chapter 4) to prepared mixed cerium titanium nanostructures

Parameters	Precipitation/hydrothermalmethod	Nanotube template method
Stirring Time	2 hrs	24 hrs
Hydrothermal temperature	150^{o}C	150^{o}C
Dwell time	48 hrs	72 hrs
HCl Treatment	No	Yes
Volume of NaOH used	8mL	80mL
Molarity of NaOH used	6M	10M
Molarity of cerium nitrate	0.1M	0.1M
Molarity of titanium oxide	0.1M	0.1M

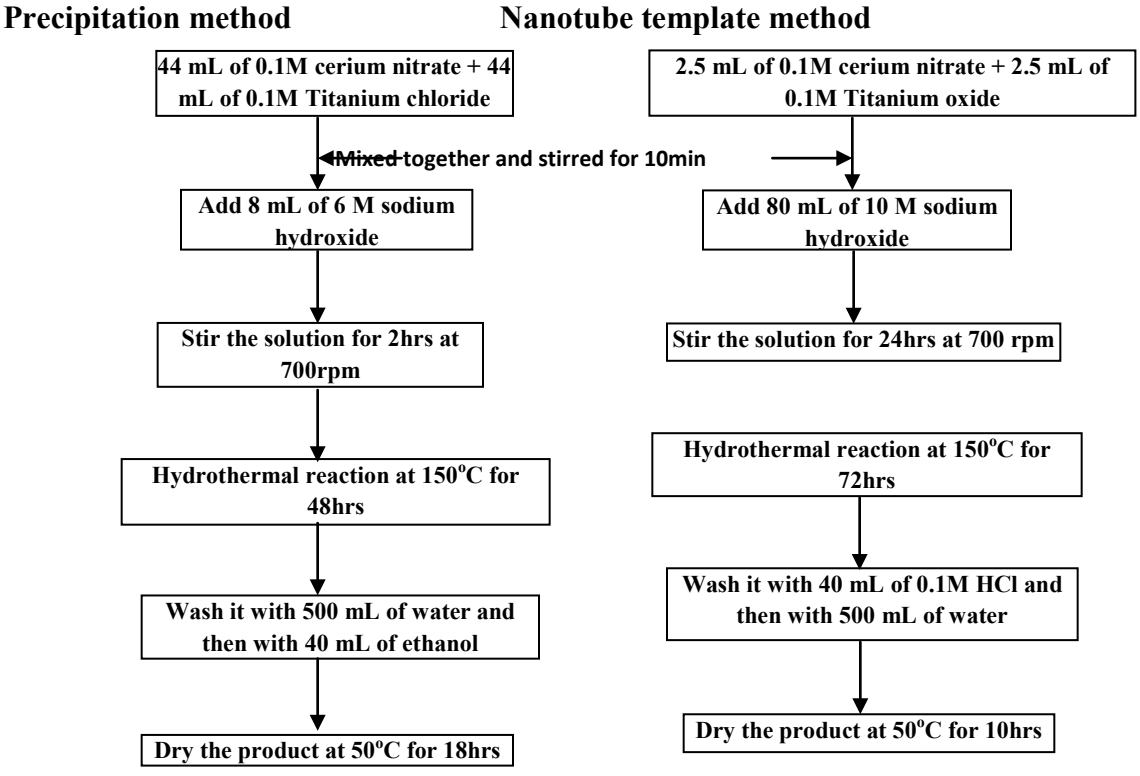

Figure 33: The flow chart comparison for the synthesis of $Ce_{0.5}Ti_{0.5}0_2$using two different methods in Chapters 3 and 4

4.2.1 P-XRD:

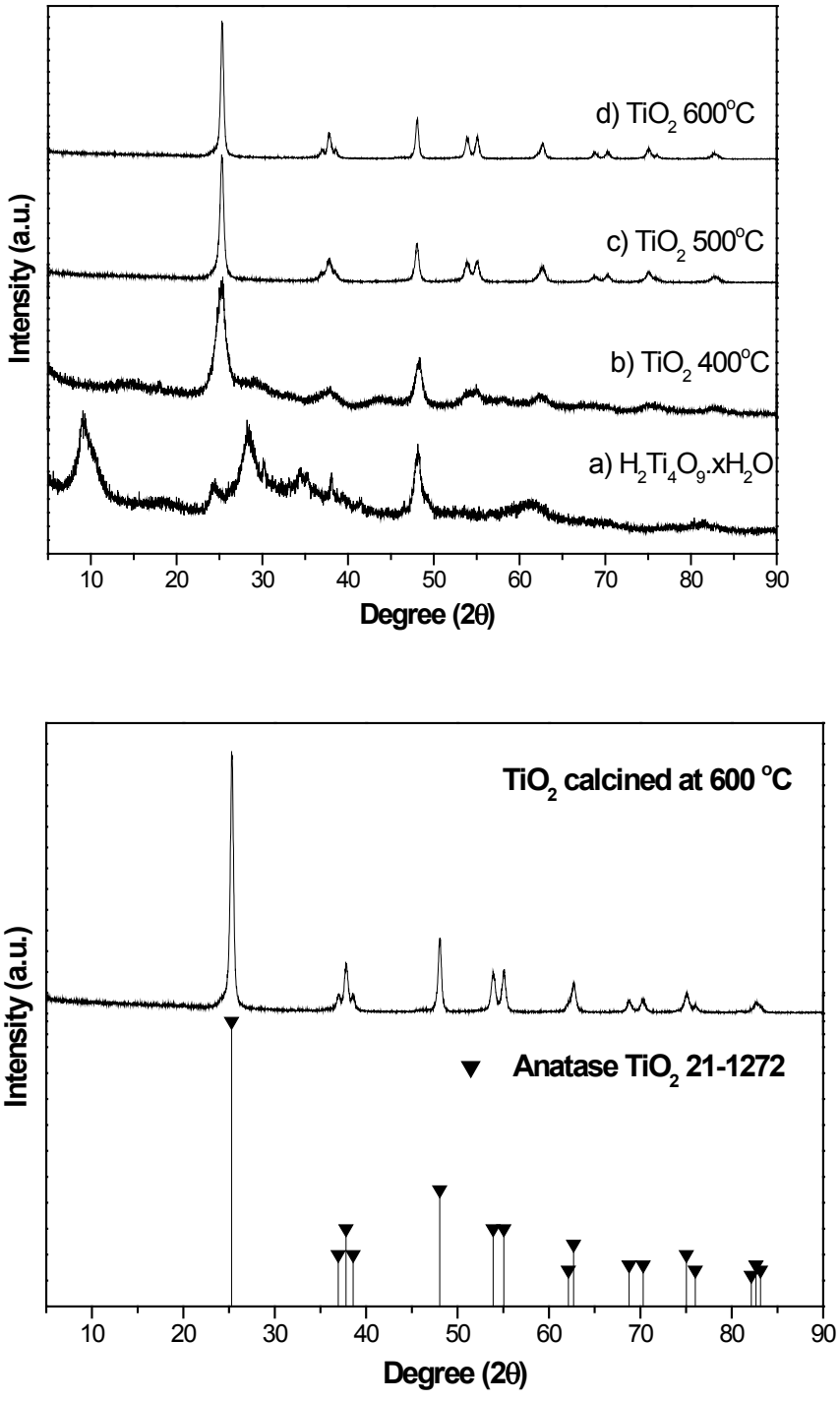

Figure 34: P- XRD plots of titanium oxide at different temperatures

Figure 34 shows the plots of the synthesized titanium oxide and the samples calcined at different temperatures. The XRD patterns revealed that the sample synthesized initially presents a hydrogen titanate phase and after thermal treatment at 600 ^{o}C, the sample was found to transform into a pure anatase phase which is confirmed using the JCPDS card No. 21-1272. All the peaks were found to be exact match. The samples were calcined at different temperatures (400, 500 and 600^{o}C)and each of them showed a significant difference in X-ray diffraction patterns.They showed broader diffraction peaks for the samples calcined at a lower temperature. The major peaks that showed significant difference with temperature are (105), (116), (215), (213), (312). Pure anatase phase was synthesized due to dehydration of hydrogen titanate with increase in calcination temperature. The crystallite size was also found to vary significantly. Usually, with an increase in calcination temperature, the crystallite size will increase gradually[42-44]. Our results were found to show the same effect. The crystallite size of each sample was calculated using scherrer equation based on the XRD data. The sample calcined at 400^{o}C showed a crystallite size of 7.4nm and the sample calcined at 500^{o}C showed 16nm and the sample calcined at 600^{o}C showed 21.6nm.

Cerium titanium mixed oxide nanostructures:

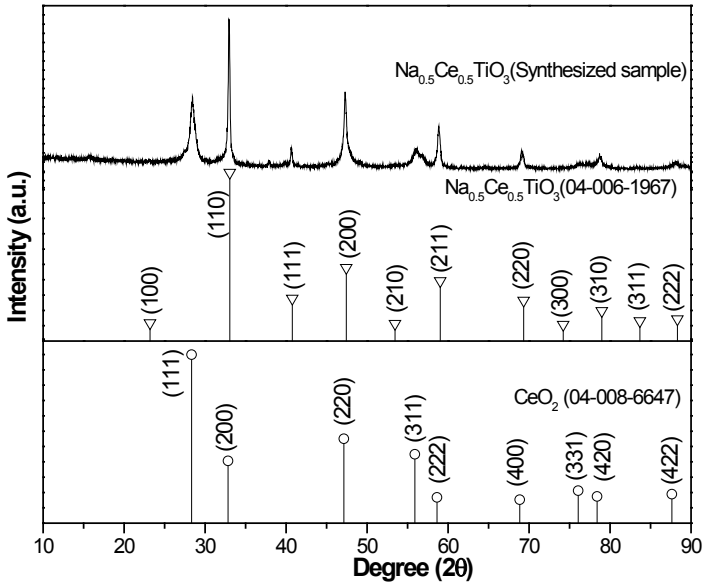

(a)

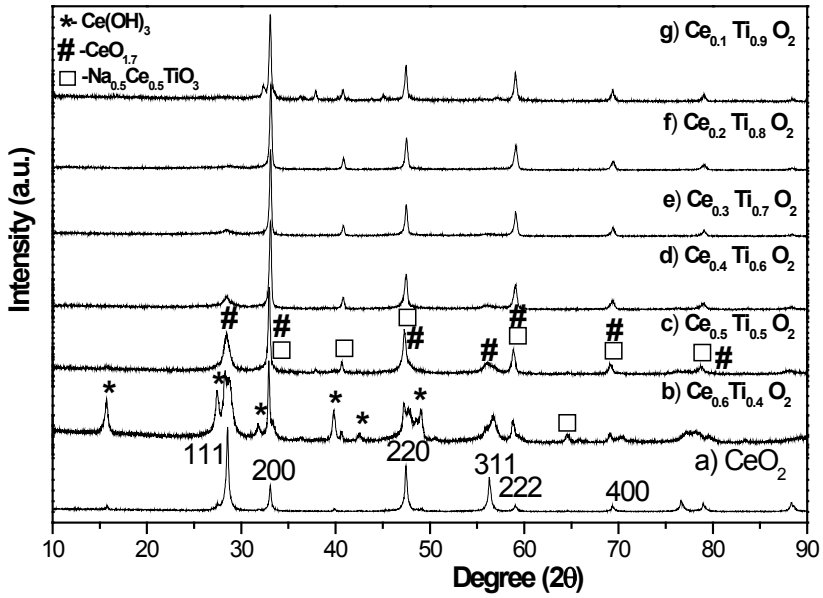

(b)

Figure 35: (a) Indexing using JCPDS (b) XRD plots of various mixed oxide samples synthesized at 150 ^{o}C

The XRD pattern shown in the Figure 35 (a) confirmed the presence of cerium oxide (JCPDS 04-008-6647) and sodium cerium titanate (JCPDS 04-006-1967) in the synthesized mixed oxide sample with a nominal composition $Ce_{0.5}Ti_{0.5}O_2$. Figure 36 (b) shows the XRD plots of various mixed oxide samples($Ce_xTi_{1-x}O_2$, x=0, 0.1, 0.2, 0.3, 0.4, 0.5, 0.6) synthesized at 150 ^oC. For a nominal composition $Ce_{0.5}Ti_{0.5}O_2$ sample, three phases (CeO_2, $Ce(OH)_3$, $Na_{0.5}Ce_{0.5}TiO_3$) were identified. The peak pattern and its individual composition for the sample $Ce_{0.5}Ti_{0.5}O_2$ was shown in Figure 37based on rietveld refinement analysis. As synthesized cerium titanium oxide also has traces of cerium oxideand cerium hydroxide. There are 9 characteristic peak that correspond to cerium oxide which are on the 2θ scale at 28.57^o, 33^o,47.60^o, 56.39^o, 59.13^o,69.51^o, 76.55^o, 78.71^o and 88.08^o correspond to (111), (200), (220), (311), (222), (400) and (331), (420), (422) planes, respectively. Some of the peaks of cerium oxide and sodium cerium titanate were found to be overlapping perfectly. The intensity of the sodium cerium titanate composition ($Na_{0.5}Ce_{0.5}TiO_3$) is very high because of its crystallinity and large particle size. The planes that correspond to sodium cerium titanate ($Na_{0.5}Ce_{0.5}TiO_3$) were (110), (111), (200), (211), (220), (300), (311), and (222). The peak at 2θ = 40.64^{o}only exists in $Na_{0.5}Ce_{0.5}TiO_3$, not in CeO_2, giving the confirmation that the synthesized samplescontain a sodium cerium titanate phase. As the contentof the cerium oxide decreases, the intensity of the cerium oxide peak corresponding to (111) plane decreasesgradually. The (111) peak of cerium oxide was almost disappeared from the peak pattern when the contentof cerium oxide reached to 30%. Due to high concentration and volume of sodium hydroxide in the starting materials, and long reaction time (72hrs (dwell time), it became possible to introduce sodium ionintothe lattice structure of cerium

titanium oxide resulted in the formation of $Na_{0.5}Ce_{0.5}TiO_3$. Various literatures revealed that crystallization of the products increases with the increase in concentration of the sodium hydroxide [46] and the same trend repeated here for our samples. The samples were found to be better crystallized with the use of 10 M sodium hydroxide than the samples synthesized using 6 M sodium hydroxide during the precipitation step.

Table 10: Crystallite size of cerium oxide, titanium oxide, cerium titanium mixed oxide

Sample composition	Crystallite size (nm)		
	130 ^{o}C sample	150 ^{o}C sample	Nanotube sample
CeO_2	9.5	6.3	31.7
$Ce_{0.4}Ti_{0.6}O_2$	6.5	5.5	38.2
$Ce_{0.3}Ti_{0.3}O_2$	7.5	2.7	46.7
TiO_2	9.9	10.4	17.3

The crystallite size of selected cerium titanium mixed oxide samples using two different methods were calculated and compared, shown in Table 10. The crystallite size of the samples using nanotube template methodincreasesdrastically compared to that of the mixed oxide samples prepared in Chapter 3.

Figure 36 revealed the presence of cerium oxide, cerium hydroxide, and sodium cerium titanium oxide based on Rietveld refinement analysis. It clearly showed that the major phaseis sodium cerium titanium oxide, $Na_{0.5}Ce_{0.5}TiO_3$.

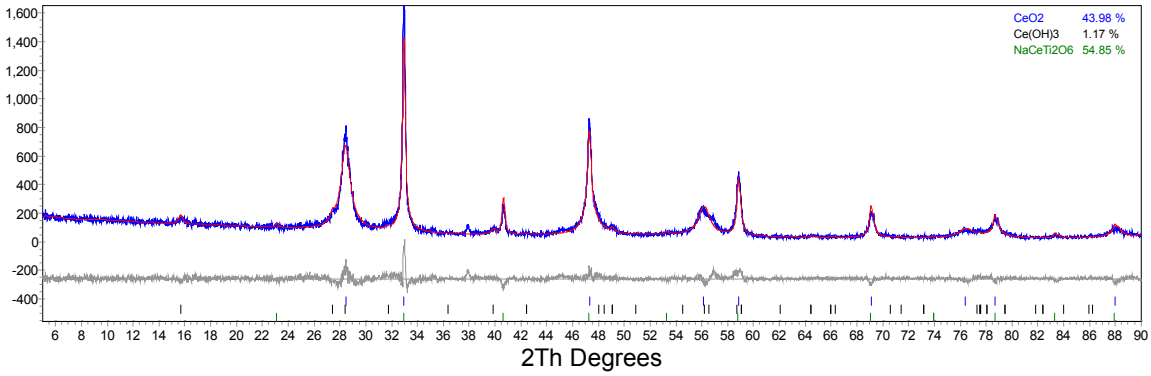
CeO2 43.98 %
Ce(OH)3 1.17 %
NaCeTi2O6 54.85 %
2Th Degrees

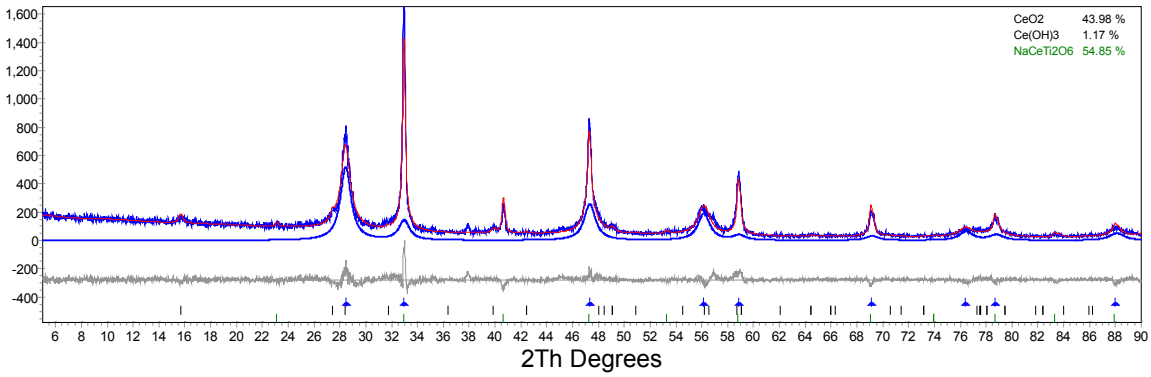
CeO2 43.98 %
Ce(OH)3 1.17 %
NaCeTi2O6 54.85 %
2Th Degrees

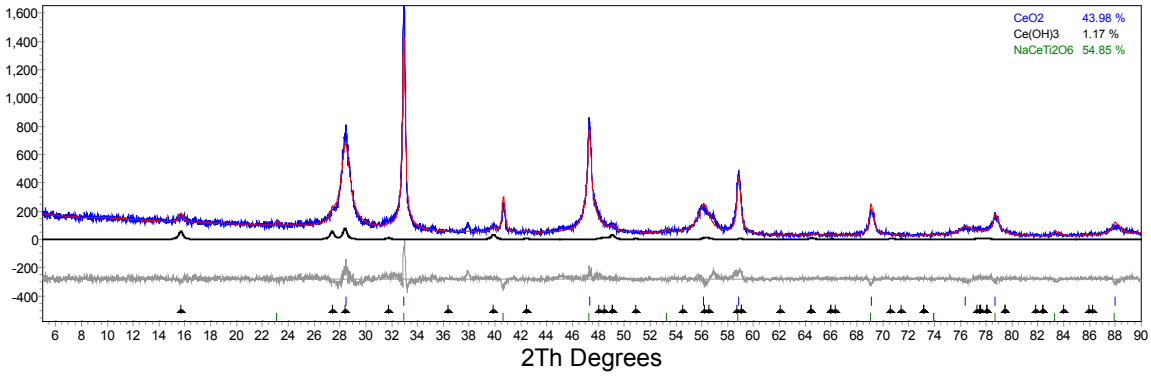
CeO2 43.98 %
Ce(OH)3 1.17 %
NaCeTi2O6 54.85 %
2Th Degrees

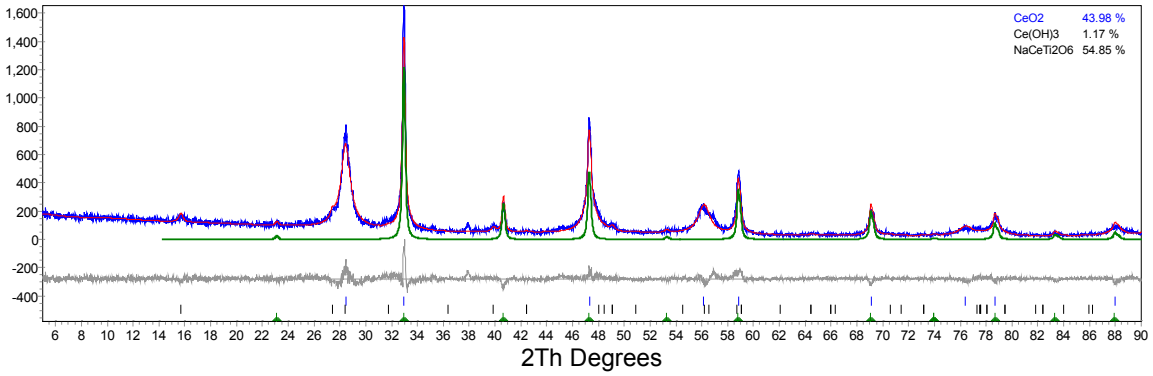

Figure 36: Phase determination using Rietveld refinement analysis

The figures starting from the second one show the presence of different phasesin the sample ($Ce_{0.5}$ $Ti_{0.5}$ O_2) synthesized. The second figure shows the presence of 43.95% of cerium oxide (CeO_2); the third one shows the presence of 1.17% of cerium hydroxide ($Ce(OH)_3$); the remaining major portion of the synthesized sample contains sodium cerium titanium oxide, $Na_{0.5}Ce_{0.5}TiO_3$.

After the successful preparation of $Ce_xTi_{1-x}O_2$mixed oxide using nanotube template method, several preliminary studies were conducted to investigate the importance of the precursors, e.g. the selection of base solution. In that, the first one was the replacement of sodium hydroxide (NaOH) with potassium hydroxide (KOH) to investigate the effect of base solution in the synthesis of $Ce_xTi_{1-x}O_2$mixed oxide nanostructures. Then we tested the possibility to prepare $Ce_xZr_{1-x}O_2$ nanostructures using the same synthesis route.

Effect of base (KOH vs. NaOH) on the formation of homogeneous Ce-Ti-O oxides:

The first preliminary study that we conducted was to identify the effect of selecting different base. Figure 37 shows XRD patterns of mixed oxide samples ($Ce_xTi_{1-x}O_2$, x=0.3, 0.4, 0.5) synthesized using two different base solutions (NaOH vs. KOH).

XRD patterns of cerium titanium mixed oxide synthesized using potassium hydroxide exhibited 13 characteristic peaks. In that 7 peaks were corresponding to potassium titanium oxide hydrate which was found at 24.41^{o}, 28.86^{o}, 30.15^{o}, 31.41^{o}, 38.36^{o}, 47.11^{o}, 56.70^{o}, 68.53^{o}. The other 6 peaks were corresponding to cerium titanium oxide and those were found at 32.51^{o}, 39.61^{o}, 40.58^{o}, 57.96^{o}, 77.71^{o}. The weak and broad diffraction patterns clearly indicate poor crystalline nature of the compounds compared to that of oxides synthesized using sodium hydroxide. With increase in the concentration of titanium oxide, the diffraction peaks at 24.41^{o} and 28.86^{o} increased gradually which corresponds to an increase in the amount of potassium titanium oxide hydrate and cerium titanium oxide, respectively. Potassium titanium oxide hydrate exhibits characteristic tetragonal phase and cerium titanium oxide exhibits cubic phase similar to fluorite structure of cerium oxide[45]. It is clear that, compared to the formation of $Na_{0.5}Ce_{0.5}TiO_3$ phase using NaOH as base solution, no $K_{0.5}Ce_{0.5}TiO_3$ was observed when using KOH, this could be due to the lager ionic size of potassium (1.38 Å), compared to that of sodium (1.02 Å).

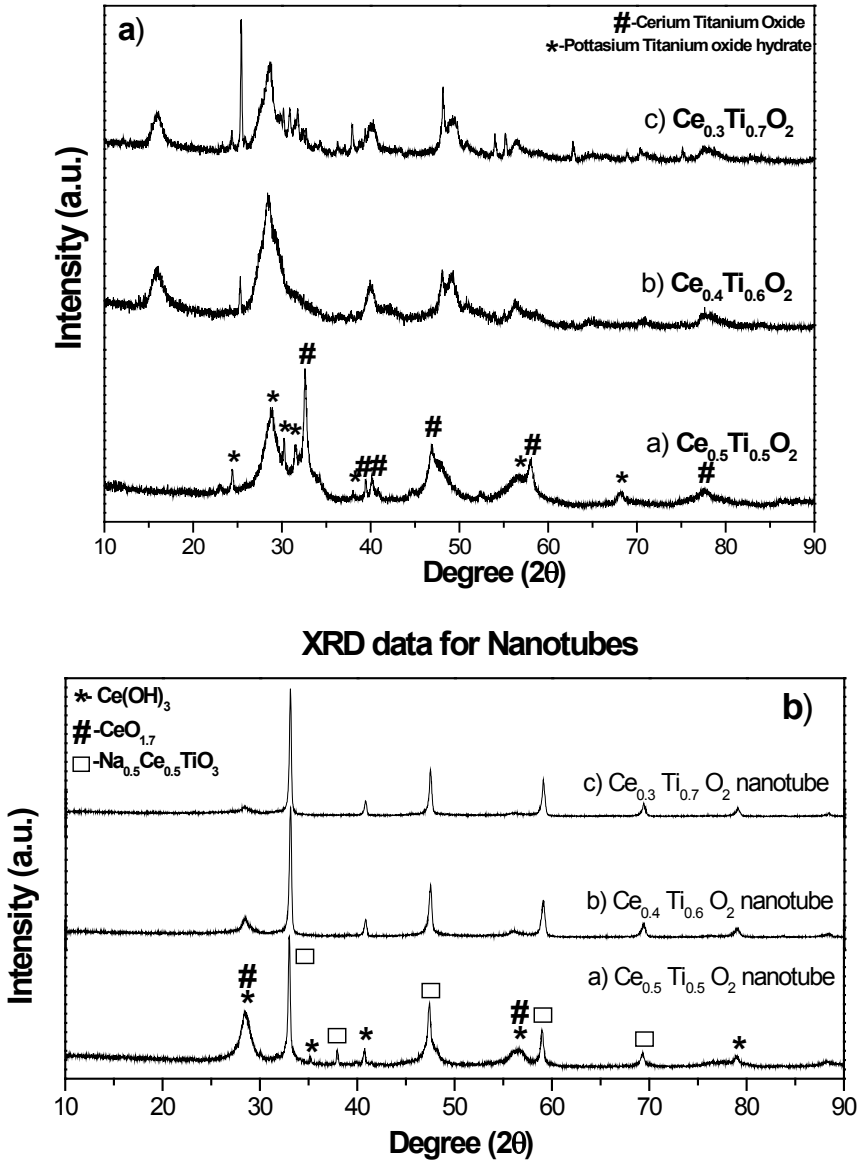

Figure 37: Plots of cerium titanium mixed oxides synthesized at 150 ^{o}C using a) KOH and b) NaOH

Synthesis of alkyl rare-earth oxide nanomaterials was found to be very innovative and revolutionary. Earlier many researchers tried to use different kind of bases. Initially they thought use of potassium hydroxide can yield better results as it is one of the strongest bases. But later it was declared that instead of being a strong base, potassium hydroxide can never yield cerium titanium mixed oxides [48]. The crystallinity of the

materials synthesized using potassium hydroxide will be very less and the X-ray diffraction patterns of the product will reflect to titanium oxide peaks. Sodium hydroxide is the best choice for the synthesis of cerium titanium mixed oxides than any other bases.

Synthesis of cerium-zirconium-mixed oxide using nanotube template method:

The second preliminary study was designed to investigate the possibility of preparing $Ce_xZr_{1-x}O_2$ using this nanotube template method.Figure 38 shows the effect of substitution of titanium oxide with zirconium oxide for the synthesis of mixed metal oxides. X-ray diffraction patterns of $Ce_{0.5}$ $Zr_{0.5}O_2$consist of 9 main reflections, 15.98^o, 27.71^o, 28.67^o, 29.93^o, 34.53^o, 40.24^o, 42.94^o, 49.44^o, 58.96^o. The diffraction peaks are characteristic of tetragonal phase of cerium zirconium oxide (JCPDS card no. 038-147) and hexagonal phase of cerium hydroxide (JCPDS card no. 074-0665). With increasing concentration of zirconium oxide, the intensity of the diffraction peak at 29.93^o gradually increases, indicating the higher amount of CeO_2-ZrO_2 solid solution.

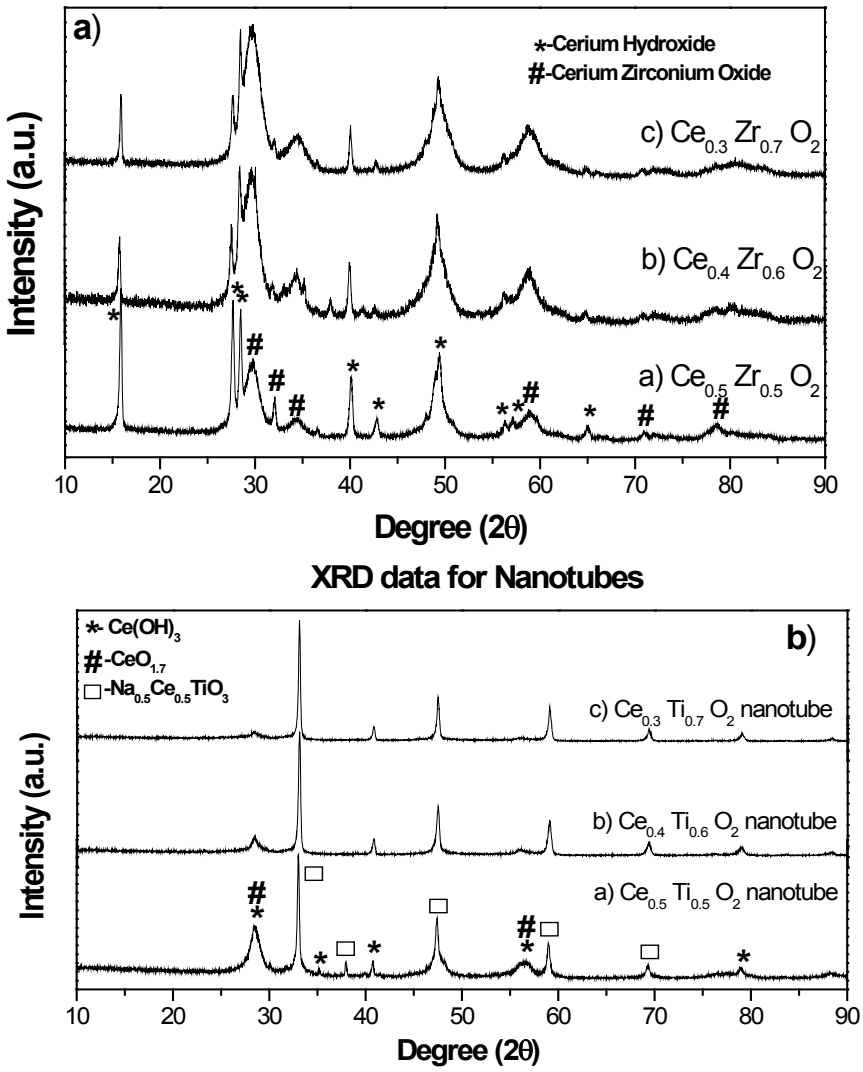

Figure 38: XRD plots of a) cerium zirconium oxide and b) cerium titanium oxide synthesized at 150 ^{o}C

Several earlier studies revealed that it is possible to synthesize cerium zirconium mixed oxide nanoparticles using hydrothermal synthesis technique [49-51]. Later it was thought that titanium oxide can form thermally more stable and better crystalline compounds than cerium zirconium oxide nanoparticles. The main reason for the hypothesis is due to the smaller ionic size of titanium (0.064nm) compared to that of zirconium (0.084nm). Due to the larger ionic size of zirconium, the lattice of ceria gets

distorted a lot more. It was clearly shown that using our nanotube template method it is possible to synthesize well defined crystalline structures of cerium titanium mixed oxide nanoparticles but it is not possible to synthesize cerium zirconium nanoparticles.

4.2.2H_2-TPR and BET surface area:

H_2-temperature program reduction analyses were conducted on Micromeritics Autochem 2920 analyzer, using a quartz U-shaped sample holder. About 0.065g-0.085g of sample was used for all the analyses and it was placed in between two small amount of the glass wool as support. Samples were analyzed between temperature range of 50-950^{o}C at a heating rate of 10^{o}C/min and the gas flow used is 5% hydrogen in argon at a flow rate of 50mL/min. The hydrogen adsorbed was detected by TCD detector.Figure 38 shows the H_2-TPR plots of $Ce_xTi_{1-x}O_2$ samples synthesized at 150 ^{o}C using thenanotube template method.

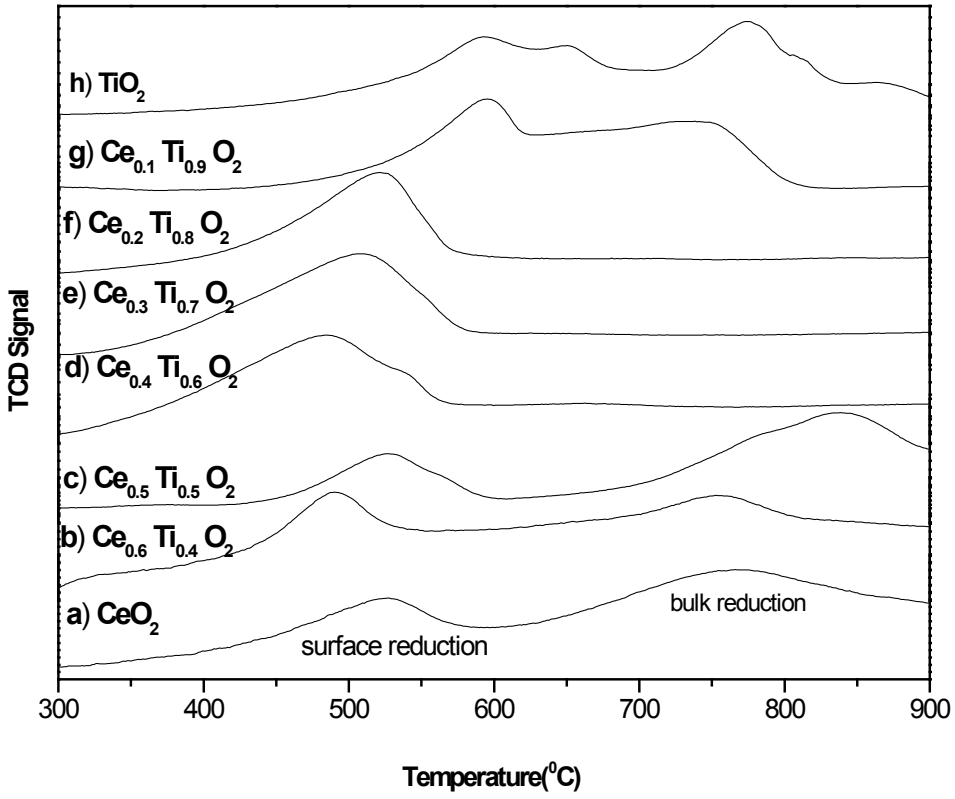

Figure 39: H_2- TPR plots of $Ce_xTi_{1-x}O_2$ samples synthesized using a nanotube template method

Figure 39 shows the H_2- TPR plots of $Ce_xTi_{1-x}O_2$ samples synthesized using a nanotube template method. The BET surface area and reduction temperature of samples with varying content of cerium oxides were analyzed and given in the Table 11 below. As discussed earlier, cerium oxide usually exhibits two reduction peaks, the low temperature peak is corresponding to the surface reduction and the high temperature peak is for thebulk reduction. For the CeO_2 sample prepared using nanotube template method, the surface reduction temperature is 527.9^oC and the bulk reduction temperature is 766.1^oC. The samples synthesized using this nanotube template method exhibited the typical reduction patterns of CeO_2. Literatures shows when titanium oxide was added even at lower concentrations to cerium oxide, it forms a perfect solid solution and will exhibit

only single reduction peak [46]. But in the current method, even though titanium oxide concentration reached to 40% it still showed weaker (111) peak of cerium oxide in the XRD analysis. This is due to the co-existence of CeO_2 and $Na_{0.5}Ce_{0.5}TiO_3$ phases in the samples. In H_2-TPR analysis, $Ce_{0.6}Ti_{0.4}O_2$ sampleshowed two reduction peaks same as cerium oxide. The surface reduction of that sample is 526 ^oC and the bulk reduction temperature is found to be 841 ^oC. The reduction temperature found to be decreased drastically by doping 50 % titanium and it still decreased by adding 60 % titanium to 483 ^oC. With the further increase in the doping concentration of titanium oxide above 70 % the reduction temperature increased but not to a greater level. Generally if both the oxides form perfect solid solution then they can enable the free movement of oxygen ions within the crystal structure which will eventually lower the reduction temperature. This movement of oxygen ions will not occur in case of pure oxides and that is the reason they always exhibit higher reduction temperatures.

Table 11: Temperature and BET surface area of $Ce_xTi_{1-x}O_2$ samples

Sample	BET surface area (m^2/g)	Reduction temperature (^oC)
CeO_2	24.70	527/766
$Ce_{0.6}Ti_{0.4}O_2$	25.75	526/841
$Ce_{0.5}Ti_{0.5}O_2$	17.40	492
$Ce_{0.4}Ti_{0.6}O_2$	18.13	483
$Ce_{0.3}Ti_{0.7}O_2$	17.25	510
$Ce_{0.2}Ti_{0.8}O_2$	16.88	517
$Ce_{0.1}Ti_{0.9}O_2$	11.46	595
TiO_2	40.36	592/774

BET:

The surface area of the samples was analyzed using Micromeritics 2920 Autochem analyzer. The surface area of cerium oxide is 24.69m^2/g, and for the sample $Ce_{0.4}Ti_{0.6}O_2$ it is 18.13m^2/g, and for $Ce_{0.3}Ti_{0.7}O_2$ it is 17.25m^2/g and forTiO_2 it is 40.36m^2/g. The surface area for all the samples is lower compared to that of mixed oxide samples using precipitation/hydrothermal method (Chapter 3). The low surface area observed may be due to the long dwell time in this method. The longer dwell time may have resulted in increase of crystallite sizes which ultimately resulted in smaller surface areas. All this data was consistent with XRD analysis.

4.2.3 Transmission Electron Microscopy:

Particle size and shape of the different samples were analyzed using the transmission electron microscope, shown in Figures 40 and 41.

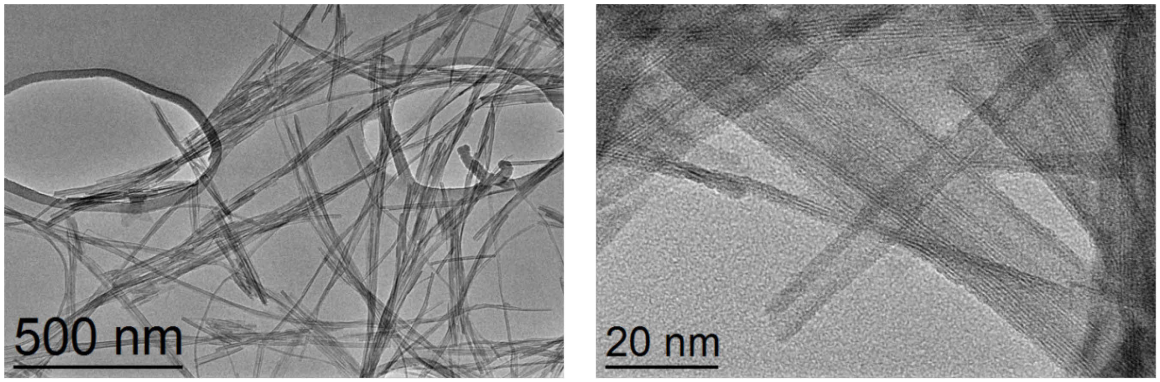

Figure 40: Low and high resolution TEM images of $H_2Ti_4O_9{\cdot}xH_2O$

Figure 40 shows low and high magnification TEM imagesof hydrogen titanate nanotube structures. At a lower magnification, they look like nanofibres, but at high

magnification it is very clear that they are nanotubes. The crystal size as calculated using XRD data was 17.3nm and the surface area obtained based on the BET analysis was 17.25m^2/g. The crystal size observed in the TEM image was found to be in good agreement with that data based on the calculations of XRD analysis.

Figure 41 shows the TEM images ofhydrogen titanate, mixed cerium titanium oxides and pure cerium oxide. In the Figure 41, image (B) shows the composition $Ce_{0.3}Ti_{0.7}O_2$ and in that as the titanium oxide was not completely substituted into the cerium oxide lattice and that can be clearly seen in the image as it was showing both cerium nanocubes and titanium nanotubes but the major ratio was of cerium oxide nanostructures. But in the image (C) it was clear that titanium oxide was substituted into the cerium lattice and that is the reason we are unable to find more of titanium oxide nanotubes. The final image shows cerium nanocubes. This nanocubes were synthesized only using this modified procedure but not with the regular mixed oxide procedure that we mentioned in our earlier chapter. The crystallite size of this mixed oxide nanostructures was found to be increased with increasing concentration of titanium oxide and consequently surface area was decreased [46].

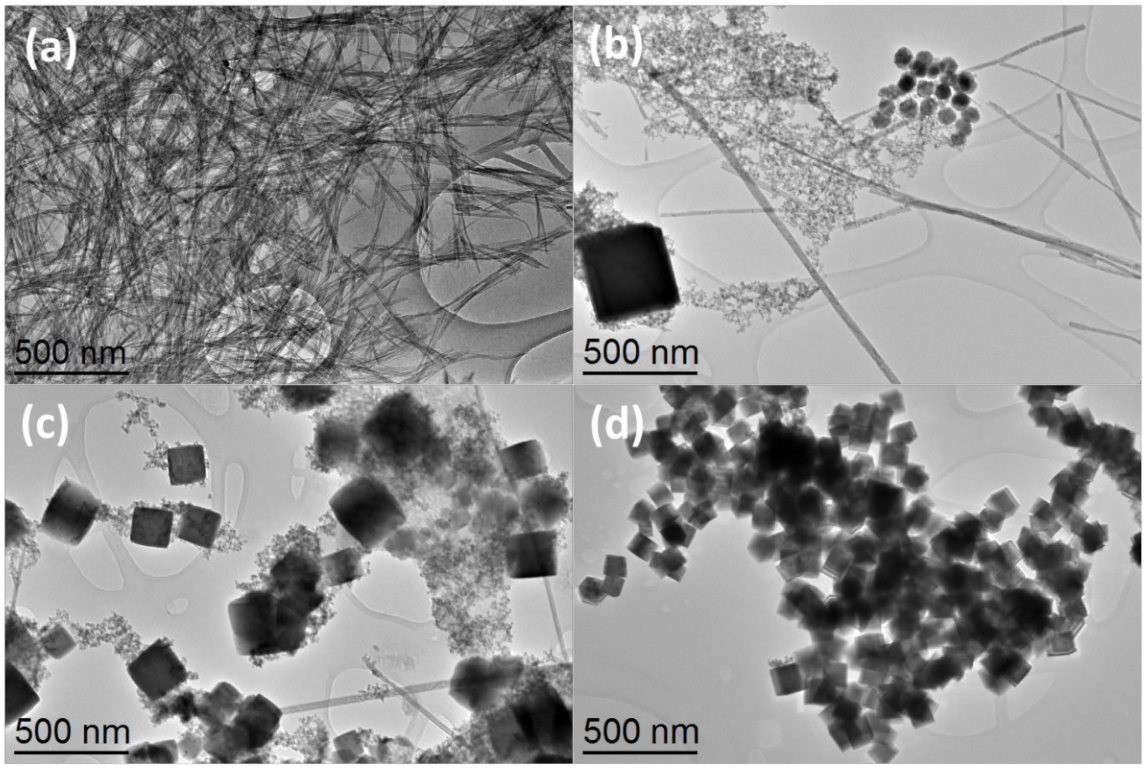

Figure 41: TEM images of (a) $H_2Ti_4O_9 \cdot xH_2O$;(b) $Ce_{0.3}Ti_{0.7}O_2$; (c) $Ce_{0.5}Ti_{0.5}O_2$; (d) CeO_2

The main goal of this project was to synthesize thermally stable, lower temperature reducible nanostructures with a high surface area and improved catalytic activity.Due to the increased crystallite size, the surface area of the materials using nanotube template method was increased drastically and is much higher compared to that of mixed oxides samples obtained in Chapter 3.

4.2.4 Raman spectroscopy

Spectroscopy data was obtained using Raman spectroscopy using a laser intensity of with a laser exposure time of 10sec for all the samples analyzed.

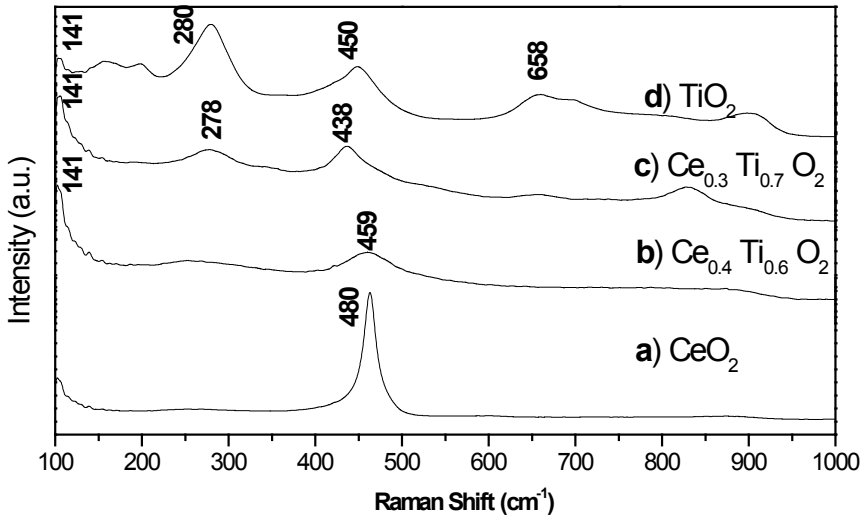

Figure 42: Raman plots of mixed oxide samples synthesized at 150 ^{o}C

The Raman scattering bands were shown in Figure 42 for the selected $Ce_xTi_{1-x}O_2$samples using the nanotube template method. Cerium oxide was found to show a strong and intense Raman scattering band at 480cm^{-1}. With the addition of titanium oxide, other peaks that are related to titanium oxide were observed. As there are many other small peaks, some are very significantly related to titanium oxide. In case of titanium oxide the Raman bands were found at 141 cm^{-1}, 280 cm^{-1}, 450 cm^{-1} and 658 cm^{-1} and this was due to the Raman active modes of titanium oxide. In them the Raman bands were seen at 141cm^{-1}, 278cm^{-1} and 438cm^{-1} for the compositions $Ce_{0.3}$ $Ti_{0.7}$ O_2 and $Ce_{0.4}Ti_{0.6}O_2$. With a higher cerium concentration in the $Ce_{0.4}Ti_{0.6}O_2$ sample, the band at 278 cm^{-1} is dismissing. The main reason for the difference was due to the substitution of titanium into the cerium lattice. For the composition $Ce_{0.3}Ti_{0.7}O_2$,the Raman bands observed mainly corresponds to those of titanium oxide indicating the perfect formation of titanium rich solid solution oxide.For the composition $Ce_{0.4}Ti_{0.6}O_2$, the Raman bands shown were similar to these bands in pure CeO_2.

4.3 Conclusions:

Synthesis of $Ce_xTi_{1-x}O_2$ ($0 \leq x \leq 1$) nanomaterials was carried out using a modified nanotube template method. Comparison experiment studies were conducted to understand the importance of base solution selection (NaOH vs. KOH) and conclude that the change in precursor or its volume or its concentration yields much different results. Thefeasibility to prepare other mixed oxide using nanotube template method was also tested.

Replacing sodium hydroxide (NaOH) with potassium hydroxide (KOH) did not give impressive results and the reason for this could be due to the larger ionic size of potassium ion than sodium ion, resulting in poor solution formation of $K_{0.5}Ce_{0.5}TiO_3$. The use of zirconium oxide instead of titanium oxide yielded the similar poor results to make cerium zirconium solid solution, indicating the importance of formation of hydrogen titanate in the method.

In order to prepare pure anatase or rutile titanium oxide, the thermal treatment study of hydrogen titanate was tested. It was found that with increasing temperature it can retain the nanotube framework and it transformed to pure anatase phase at 600 ^oC.

In comparison with the results in Chapter 3 using the precipitation/hydrothermal method,the crystallite size of the synthesized nanoparticles is much larger and the BET surface area is lower.The reduction temperaturedetermined by H_2-TPRis similar to the samples prepared using the precipitation/hydrothermal method; however the larger particle size with a similar reduction temperature indicates that the synthesized nanostructures have better activity. Further studies will be focused on obtaining higher

surface area nanoparticles, loading 1wt% Pt or Au onto these oxide supports and testing their catalytic activity for CO oxidation reaction.

CHAPTER 5: Synthesis of graphene oxide-supported CeO_2/ TiO_2 nanocomposites

Graphene oxide is a highly oxygenated form of graphene which readily gets exfoliated in water and forms stable dispersions. Graphite has been used as precursor for the synthesis of graphene oxide by oxidation and subsequent dispersion and exfoliation in water. Earlier mechanical exfoliation and epitaxial chemical vapor deposition techniques were employed for the synthesis of graphene oxide. But the major disadvantage of these methods was they were not efficient for large scale manufacturing. First one to demonstrate the synthesis of graphene oxide is Brodie in 1859. He used potassium chlorate ($KClO_3$) as an oxidizing agent instead of potassium permanganate ($KMnO_4$) that is used widely in the recent years [58]. Later, Staudenmaier in 1898 made some modifications to the Brodie procedure and did the graphene oxide (GO) synthesis. Staudenmaier used both concentrated sulfuric acid and nitric acid instead of just nitric acid as in Brodie's procedure and he also added the oxidizing agent, potassium chlorate in certain intervals instead of adding it all at once. These small changes yielded in synthesizing the graphene oxide (GO) in a single reaction vessel [59]. Finally, Hummer in 1958 reported the most frequently used procedure in now days. He made some major modifications. Hummer used potassium permanganate as an oxidizing agent instead of potassium chlorate that is used by earlier researchers. Hummer also used sodium nitrate along with $KMnO_4$ [60]. Graphene oxide is very hydrophilic nature due to the presence of polar oxygen functional groups. Due to its strong hydrophilic nature it can be easily dispersed and exfoliated in water [61]. Graphene oxide can be uniformly deposited on the substrates and that is possible only due to its hydrophilic nature. The common source of graphite that is used in synthesizing graphene oxide is flake graphite.

There are a lot of assumptions on the structure of graphene oxide. The precise atomic structure of graphene oxide is still remaining unexplained due to its nonstoichiometric atomic composition and also due to the presence of covalent oxygenated functional groups [62]. Many assume that graphene oxide has a single layer structure.

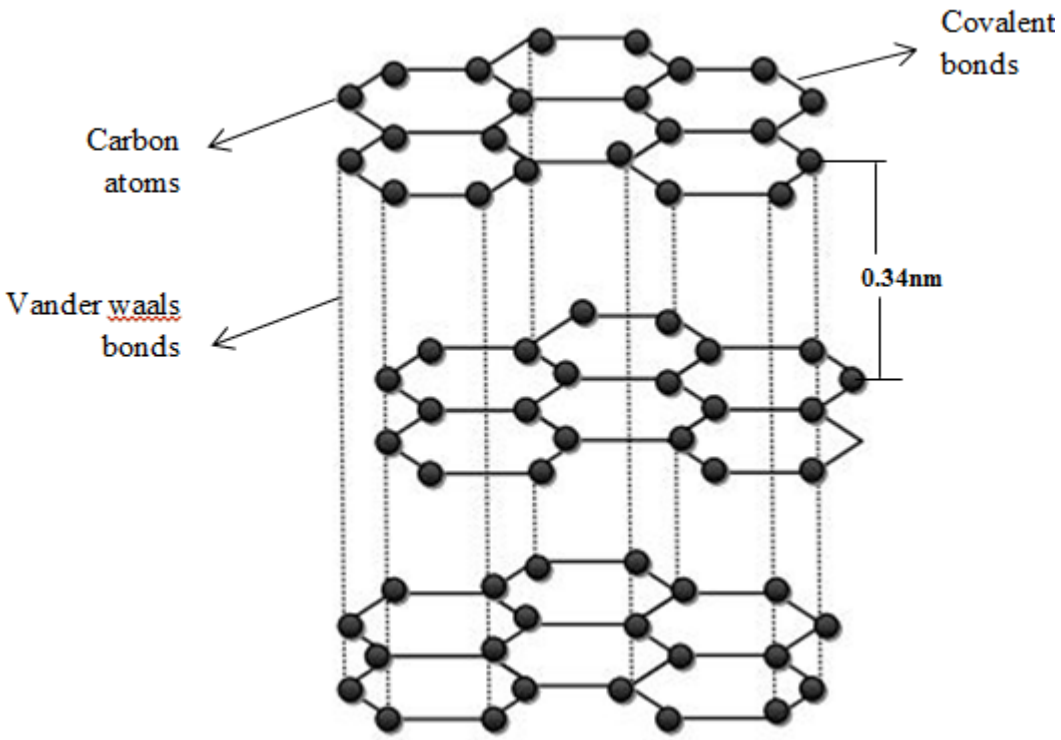

Figure 43: Structure of graphite oxide

As discussed earlier the precise structure of graphene oxide is still unknown. Figure 43 shows the estimated structure of graphite. There are some assumptions made by some of the researchers earlier based on their research findings. The structure of graphene oxide on a basic level can be explained as dispersion of oxygen atoms on both basal planes and edges around graphene sheets. Hoffman and Holst [63] in 1939 thought that graphene oxide may contain modified planar carbon layers due to epoxy group and

also proposed that the molecular formula might be C_20. Ruess [64] in 1946 proposed that the structure of graphene oxide is not only planar but also puckered and according to his assumption the functional groups that are around the planar carbon layers are hydroxyl and ether like oxygen bridges. Scholz and Boehm [65] in 1969, proposed a structure that is supposed to have a corrugated carbon layers. They assumed that the functional groups around the carbon sheets were carbonyl and hydroxyl groups instead of epoxide and ether groups. Nakajima et al., [66] proposed something different compared to other scientists. He suggested that there will be two carbon layers that are linked by sp^3 carbon-carbon bonds and the functional groups that are thought to be present are carbonyl and hydroxyl groups. Based on all the assumptions it is very clear that all the structural proposals were made purely based on graphite oxide. In general, the graphene oxide will have large amount of sp^2 hybridized carbon atoms and smaller amount of sp^3 hybridized carbon atoms. The sp^3hybridized carbon atoms are bonded with oxygen functional groups and that is the reason they are considered are oxidized regions and the sp^2 hybridized regions are considered as unoxidized regions due to the absence of oxygen functional groups.

The graphene oxide tends to have a varied number of properties. The properties of graphene oxide such as conductivity is strongly reflects to its chemical and atomic structures. The electrochemical, electronic and mechanical properties of graphene oxide strongly depend on the type of oxygenated groups present around the carbon layers. Graphene oxide can also be used as semi metallic, semi conducting or insulating materials by altering the oxidation or reduction parameters. Due to the enhanced electrochemical properties the interest on graphene oxide based materials has increased a lot now days.

5.1 Synthesis procedure:

As explained earlier, in the recent days Hummers method is used widely for the synthesis of graphene oxide. In our study we used slightly modified Hummers method. We used 2g of graphite powder and digested initially using 45mL of sulfuric acid, stirred continuously for 15min and then cooled using ice water bath. Meanwhile,5.5g of strong oxidizing agent,thepotassium permanganate ($KMnO_4$) was addedgradually with continuous stirring. The reaction mixture was still kept in ice water bath to avoid overheating. The reaction mixture was stirred for 15 min and then it is removed from ice water bath. It was then stirred continuously for 2 hrs at room temperature. Then 92 mL of water was added slowly, followed by addition of 250 mL of hydrogen peroxide and finally it was stirred for 25 min and then filtered and washed with 500 mL of 10% hydrochloric acid. The obtained filtrate was dispersed and exfoliated in water to obtain stable graphene oxide sheets. It was filtered again andthe final product was dried at 50^oC for 8 hrs [67].

The synthesis procedure is shown using flow chart below in Figure 44.

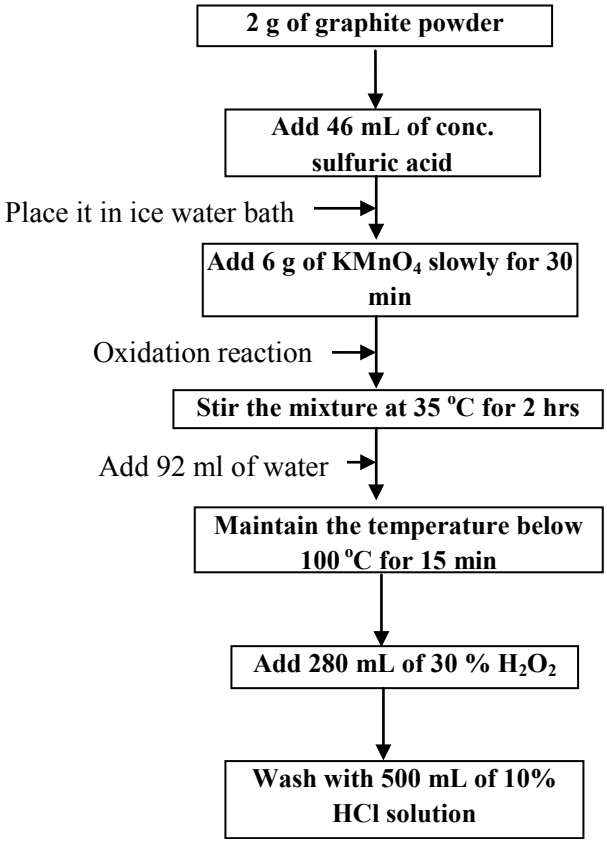

Figure 44: Flow chart for the synthesis of graphene oxide

The synthesis procedure of cerium/titanium graphene oxide nanocomposites varies with that of regular graphene oxide synthesis. In our study we used nanotube template method for the mixed oxide/graphene oxide synthesis. The graphene oxide was added to sodium hydroxide along with cerium/titanium oxide and stirred for 24 hrs. Further synthesis procedure was just the same as nanotube template method which was already explained in Chapter 4.

The basic schematic of synthesis of graphene oxide and graphene oxide based mixed oxides nanocomposites are shown in Figure 45.

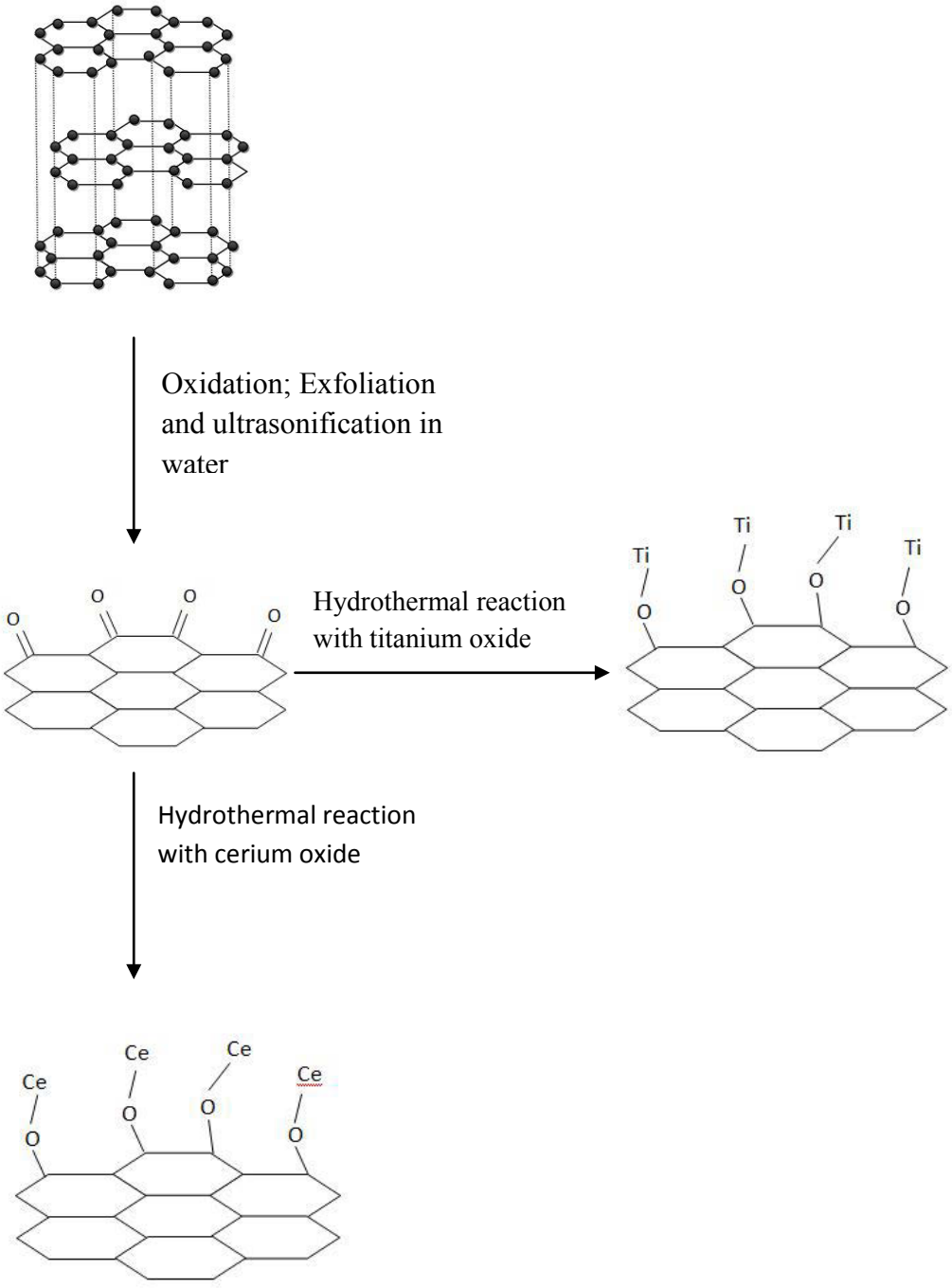

Figure 45: Schematic of synthesis of graphene oxide and cerium/titanium graphene oxide.

Oxidation of graphite with strong oxidizing agent like potassium permanganate ($KMnO_4$) and by further exfoliation and ultrasonication yields graphene oxide. Hydrothermal treatment of graphene oxide with cerium/titanium oxide at 150 ^oC yielded cerium/titanium graphene oxide. The sample was characterized using Rigaku Miniflex X-ray diffraction.

5.2 Sample characterization:

XRD characterization for this study was carried on Rigaku instrument with a scan speed of 0.5^o /min in the 2θ range of 5^o-95^o equipped with Cu-Kα radiation.

5.2.1 Characterization of graphene oxide:

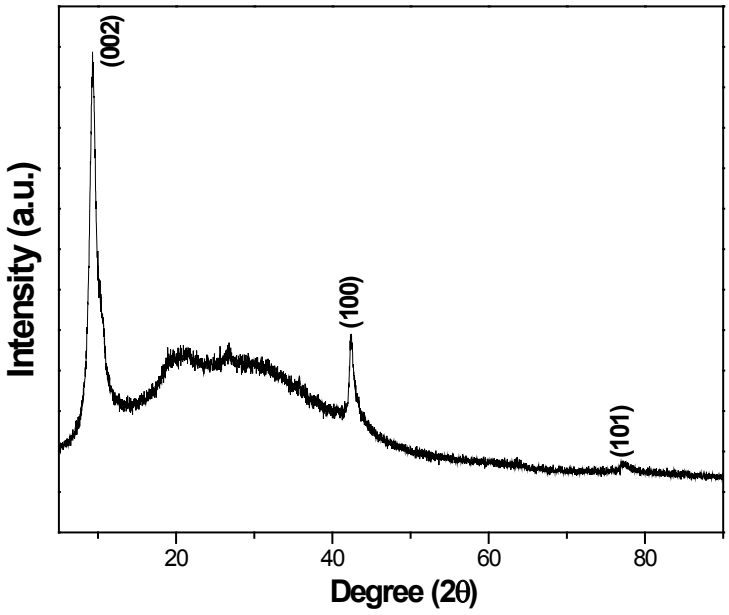

Figure 46: P-XRD plot of graphene oxide

The XRD pattern of graphene oxide (GO) in Figure 46 shows a strong peak at 2θ = 10.8^o corresponds to interlayer distance of 5.8 Å (d_{002}). The interlayer distance was calculated using scherrer's equation. The XRD pattern also shows two weak peaks at 2θ

= 42.2° and 77.2° corresponds to interlayer distance of 2.7 Å(d_{100}) and 7.05 Å(d_{101}) respectively. Generally the interlayer distance of graphene oxide will be always greater than that of graphite. The interlayer distance range of the graphite is 2-4 Å and for graphene oxide it is between 5-9 Å [68]. This difference is due to the presence of defects in the structure and also due to the presence of nanoholes. The presence of intercalated water molecules and various oxides were also the reason for this larger interlayer distance for graphene oxide.

5.2.2 Characterization of cerium- graphene oxide**:**

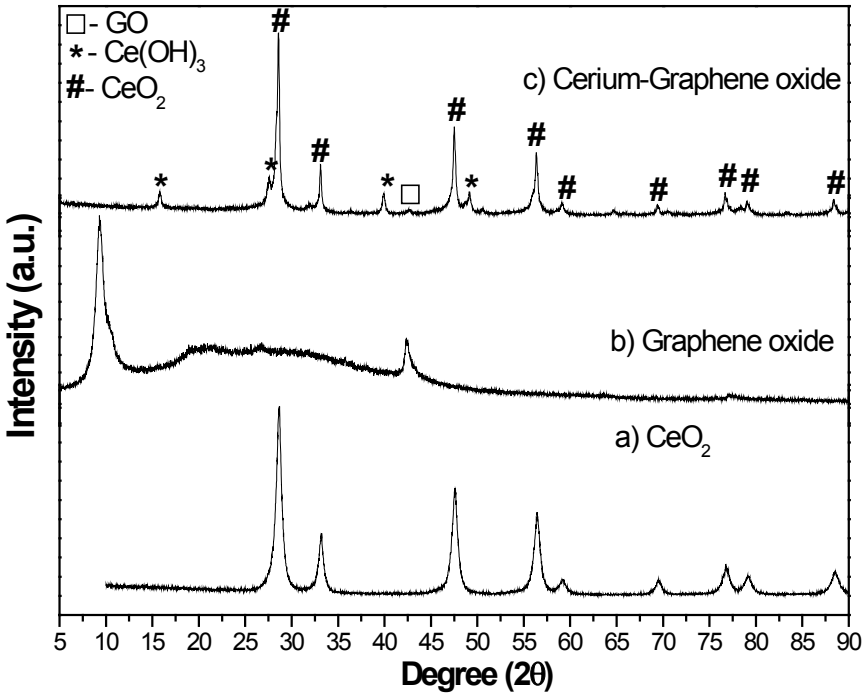

Figure 47: P-XRD plot of ceria-graphene oxide nanocomposites

Figure 47 shows the XRD patterns of ceria graphene nanocomposites. The XRD pattern showed exhibited peaks at 15.6°, 27.4°, 28.4°, 33°, 39.8°,42.4°, 47.4°, 49°, 56.2°, 59°, 69.3°, 76.6°, 79°, 88.3°. The diffraction peak at 42.4° corresponds to graphene

oxide.All the other peaks exceptthe peaks at 27.4^{o},15.6^{o}, 39.8^{o}, 49^{o}correspond to cubic fluorite cerium oxide (JCPDS 34-0394). The exceptional peaks correspond to hexagonal cerium hydroxide (55-0556). The peak patterns indicated that the as synthesized material was highly crystalline. By this XRD patterns it can be concluded that in this synthesis process along with cerium oxide and graphene oxide, cerium hydroxide was also synthesized. The majority of the peaks correspond to cerium oxide with a shorter and weak peak of graphene oxide shown due to slight stacking of graphene nanosheets [69-70]. This is mainly due to the reduction of graphene oxide during hydrothermal process [69]. The reduced graphene oxide has more advantages than graphene oxide.

5.2.3 Characterization of titanium oxide-graphene oxide nanocomposites:

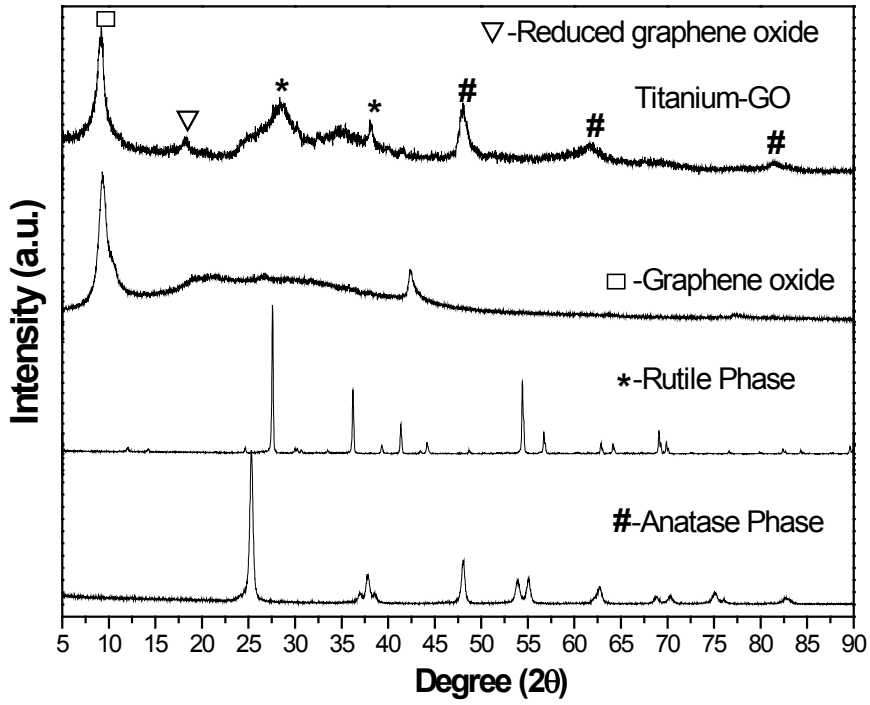

Figure 48: P- XRD plot of titanium oxide graphene oxide nanocomposites

The XRD pattern of titanium oxide graphene oxide was shown in Figure 48. The majority of the peaks shown in Figure 48 correspond to anatase phase. The peaks that correlated with anatase phase were found at $2\theta = 47.9^{o}$, 61.5^{o}, 81.4^{o}. The peaks at $2\theta = 28.3^{o}$, 38^{o} were correspond to rutile phase titanium oxide. The remaining peaks were one at 9.1^{o} correspond to graphene oxide and peak at 18.1^{o} correspond to reduced graphene oxide. This synthesis helped in the synthesis of both anatase phase titanium oxide and reduced graphene oxide. Both the products have individually have many important applications but by adding titanium oxide support to reduced graphene oxide the properties of both the compounds are enhanced such as the catalytic activity of titanium oxide will be enhanced and the photoluminescence property of graphene oxide was also increased. The peaks of graphene oxide were found to broader and weaker. This is due partial reduction of graphene oxide during hydrothermal reaction. As specified earlier the reduced graphene oxide has enhanced properties than graphene oxide. The lattice constant of titania/graphene oxide nanocomposites may increase if the Ti^{+4} converts to Ti^{+3} as the ionic size of Ti^{+3} is larger than that of Ti^{+4} [71] (ionic size of Ti^{3+}- 0.670 Å and ionic size of Ti^{4+}- 0.605 Å).

5.3 Conclusions:

It can be concluded that it is possible to synthesize CeO_2/graphene oxide and TiO2/graphene oxide nanocomposites using nanotube template method.

CHAPTER 6: Conclusion

Our research goal was to synthesize nanostructures with larger surface area, smaller particle size and lower temperature reducibility and also with higher thermal stability.

We used two different methods to reach our goal. One is precipitation method and the other one is nanotube template method. In our Chapter 3 we discussed about the precipitation method and in Chapter 4 we discussed about the nanotube template method.

In chapter 3 we synthesized cerium oxide, titanium oxide and cerium titanium mixed oxides using precipitation/hydrothermal method. As stated earlier the main goals of the project were to synthesize nanomaterials with better thermal stability, higher surface area and lower temperature reducibility. Materials with higher surface area (126.9 m^2/g) and better temperature reducibility (466 ^oC) were synthesized.

The only major problem with the precipitation method was we are unable to synthesize shape-controlled and thermally stable compounds. Nanomaterials tend to have more thermal stability and better activity than the mixed oxides. In particular it was stated by many researchers that the nanomaterials having alkaline nature will exhibit better thermal stability than regular nanomaterials. So, we have decided to synthesize nanomaterials having a sodium element substituted into their lattice.

We made some slight modifications to this precipitation procedure in order to overcome these problems. This lead to the use of nanotube template method to overcome this problems and this can be discussed in the later chapter.

In Chapter 4 synthesis of $Ce_xTi_{1-x}O_2$ ($0 \leq x \leq 1$) nanomaterials was carried out using a modified nanotube template method. Preliminary studies were conducted to understand the importance of base solution selection (NaOH vs. KOH) and conclude that the change in precursor or its volume or its concentration yields much different results. Thefeasibility to prepare other mixed oxide using nanotube template method was also tested.

Replacing sodium hydroxide (NaOH) with potassium hydroxide (KOH) did not give impressive results and the reason for this could be due to the larger ionic size of potassium than sodium, resulting in poor solution formation of $K_{0.5}Ce_{0.5}TiO_3$. The use of zirconium oxide instead of titanium oxide yielded the similar results to make cerium zirconium solid solution, indicating the importance of formation of hydrogen titanate.

In order to prepare pure anatase or rutile titanium oxide, the thermal treatment study of hydrogen titanate was tested. It was found that with increasing temperature it can retain the nanotube framework and it transformed from mixed phase to pure anatase phase at 600 ^oC.

In comparison with the results in Chapter 3 using the precipitation/hydrothermal method, the crystallite size of the synthesized nanoparticles is larger and the BET surface area is lower. The reduction temperature determined by H_2-TPRis similar to the samples prepared using the precipitation/hydrothermal method, however the larger particle size with a similar reduction temperature indicates that the synthesized nanostructures have better activity.

Our future studies will be focused on obtaining higher surface area nanoparticle and loading 1wt% Pt or Au onto this oxide support and testing the catalytic activity of CO oxidation reaction.

References:

1. J.A. Rodriguez, X. Wang, J.C. Hanson, G. Liu, A. Iglesias Juez, *J. Chem. Phys.,* **(2003),** *119,* 5659
2. J.A. Rodriguez, X. Wang, J.C. Hanson, G. Liu, A. Iglesias Juez, *J. Chem. Phys.,* **(2004),** *121,* 5434
3. L.G.H. Pfalzgraf, C. Sirio, C. Bois, *J. Polyhedron,* **(1998),** *17,* 821
4. C. Lamonier, A. Ponchel, A. D'Huysser, L.J. Duhamel, *J. Catalysis Today.,* **(1999),** *50,* 247
5. G. Zhou, P.R. Shah, R.J. Gorte, *Catalysis letters.,* **(2004),** *120,* 191
6. A.E. Nelson, K.H. Schulz, *J. Appl. Surface Science.,* **(2002),** *210,* 206
7. T.masui, H.hirai, N.imanaka, G.adachi.,*Material Science Letters,* (2002), *21,* 489
8. H. Masanori, K. Etsuro, *J. Am. Ceram. Soc*., 82, **(1999)**, *3,* 786
9. J. Fang, B. Xinzhen, S. Dejun, J. Zhiquan, H. Weixin, *J. Appl. Surface Science.,* **(2007),** *253,* 8952
10. S. Watanabe, M. Xiaoliang, S. Chunshan, *J. Phys. Chem.,* **(2009),** *113,* 14249
11. P.S. Maria, V.R. Mastelaro, P.A.P. Nascente, A.O. Florentino, *J. Phys. Chem.,* **(2001),** *105,* 10515
12. X. Gao, Y. Jiang, Y. Fu, Y. Zhong, Z. Luo, K. Cen, *Catalysis Communications.,* **(2010),** *11,* 465
13. Y.Quan, D. Hao-Hong, L. Le-Le, S. Ling-Dong, Z. Ya-Wen, Y. Chun-Hua, *J. Colloid and Interface science.,* **(2009),** *335,* 151
14. J.C. Summers and S.A. Ausen, *J. Catal.,* **(1979),** *58,* 131
15. G. Kim, *J. Ind. Eng. Chem. Prod. Res. Dev.,* **(1982),** *21,* 267

16. B.T. Kilbourn, *J. Less Common Metals.,***(1986),** *126,* 101

17. U. Diebold, *J. Appl. Phys.,* **(2002),** *76,* 1

18. H.J. Freund, *J. Ind. Ed. Engl.,* **(1997),** *36,* 452

19. C.T. Campbell, *J. Surf. Sci. Rep.,* **(1997),** *27,* 1

20. A. Trovarelli, *J. Catal. Rev. Sci. Eng.* **(1996),** *38,* 439

21. A. Preuss, R. Gruehn, *J. Solid State Chem.,* **(1994),** *110,* 363

22. .G.W. Morey and P. Niggli; *J. Am. Chem.Soc.,* (1913), *35,* 1086

23. R.A. Laudise; *J. The growth of single crystals.,*(1970), 278

24. A. Rabenau; *J. Angew. Chem.,* (1985), *24,* 1026

25. A.N. Lobachev; *J. Crystallization processes under Hydrothermal conditions.,*(1973), 155

26. R. Roy; *J. Solid state chem., (1994), 111,* 11

27. K. Byrappa; *J. Hydrothermal growth of crystals.,*(1992), 25

28. M. Yoshimura and H. Suda; *J. Hydroxyapatite and Related Materials.,*(1994), 45

29. R.W. Henley; *J. Chem. Geol.,* (1973), *11,* 73

30. P.M. Dove and D.A. Crerar; *J. Geochim.Cosmochim.Acta.,(*1990*), 54,* 955

31. P.M. Fenn; *J. Can. Mineral.,* (1977), *15,* 135

32. W. Freidrich, P. Knipping and M. Von Laue; *J. Proc. Bavarian Acad. Sci., (*1912*),* 303

33. R.Narayanan and R.M. Laine; *J. Appl. Organomet. Chem.,* (1997), *11,* 919

34. X. Liu and W.Yu; *J. Applied polymer science.,*(2006), *99,* 937

35. J. Buckingham; *J. British journal of applied Physics.,*(1965), *16,* 12

36. R. Henderson; *J.Q. Rev. Biophys.,* (2004), *37,* 3

37. M.P. Francisco, V.R. Mastelaro, A.P. Nascente, A.O. Florentino, *J. Phys. Chem.* (**2001**), *105,* 10515

38. N. Takezawa, N. Iwasa, *J. Catal. Today,* **(1997),** *36,* 45

39. P. Larsson, A. Andersson, *J. Appl. Catal.* **(2000),** *24,* 175

40. P. Larsson, A. Andersson, *J. Catal.* **(1998),** *179,* 72

41. K. Kosuge, P.S. Singh, *J. Phys. Chem.* **(1999),** *103,* 3563

42. J.R. Davis, Z. Liu, *J. Chem. Mater,* **(1997),** *9,* 2311

43. S. Watanabe, X. Ma, C. Song, *J. Phys. Chem.* **(2009),** *113,* 14249

44. N.V. Skorodumova, S.I. Simak, B.I. Abrikosov, B. Johansson, *J. Phys. Rev. Lett.* **(2002),** *89,* 166601

45. V.E. Henrich, G. Dresselhaus, H.J. Zeiger, *J. Phys. Rev. Lett.* **(1976),** *36,* 1335

46. H.C. Yao, Y.F.Y. Yao, *J. Catal.* (**1984**), *86,* 254

47. B.M. Reddy, A.Khan, *J. Catal. Rev.-Sci. Eng.* **(2005),** *47,* 257

48. M.P. Francisco, V.R. Mastelaro, A.P. Nascente, A.O. Florentino, *J. Vac. Sci. Technol.* **(2001),** *19,* 1150

49. B. Poudel, W. Wang, C. Dames, J. Huang, S. Kunwar, D. Wang, D. Barnerjee, G. Chen, Z. Ren, *J. Nanotechnology,* **(2005),** *16,* 1935

50. D. Seo, H.Kim, J. Lee, *J. Crystal Growth,* **(2005),** *275,* 2371

51. M. Wei, Y. Konishi, H. Zhou, H. Sugihara, *J. Solid State Commun.,* **(2005),** *133,* 493

52. A. Kukovecz, M. Hodos, E. Horvath, G. Radnoczi, Z. Konya, I. Kiricsi, *J. Phys. Chem.* **(2005),** *109,* 17781

53. S. Zhang, J. Zhou, Z. Zhang, Z. Du, A. Vorontsov, J. Zhensheng, *J. Chin. Sci. Bull.* **(2000),** *16,* 1533

54. Z. Yuan, B. Su *J. Chem. Phys. Lett.* **(2002),** *363,* 362

55. I. Park, S. Jang, J. Hong, R. Vittal, K. Kim, *J. Chem. Mater.* **(2003),** *26,* 4633

56. X. Gao, H. Zhu, G. Pan, S. Ye, Y. Lan, F. Wu, D. Song, *J. Phys. Chem.,* **(2004),** *108,* 2868

57. B.M. Reddy, A.Khan, *J. Catal. Rev.-Sci. Eng.* **(2005),** *47,* 257

58. M.P. Francisco, V.R. Mastelaro, A.P. Nascente, A.O. Florentino, *J. Vac. Sci. Technol.* **(2001),** *19,* 850

59. B.C.Brodie, *J. Philos. Trans. R. Soc. London,***(1859),** *14,* 249

60. L. Staudenmaier, *J. Ber. Dtsch. Chem. Ges,* **(1898),** *31,* 1481

61. W.S. Hummers, R.E. Offeman, *J. Am. Chem. Soc.,* **(1958),** *80,* 133

62. O.C. Compton, S.T. Nguyen, *J. Adv. Mater.,* **(2010),** *22,* 711

63. B. Brodie, *J. Ann. Chim. Phys.* **(1860),** *59,* 466

64. U. Hoffman, R. Holst, *J. Ber. Dtsch. Chem. Ges.,* **(1939),** *72,* 754

65. G. Ruess, *J. Monatsh. Chem.,* **(1946),** *76,* 381

66. W. Scholz, H.P.Z. Boehm, *J. Anorg. Allg. Chem.,* **(1969),** *369,* 327

67. T. Nakajima, Y. Matsuo, *J. Carbon.,* **(1994),** *32,* 469

68. Z.Q. Li, C.J. Lu, Z.P. Xia, Y. Zhou, Z. Luo., *Carbon.,* **(2007),** *45,* 1686

69. J. Linhai, Y. Mingguang, L. Bo, L. Quanjun, L. Ran, L. Hang, L. Shuangchen, G. Chen, Z. Bo, C. Tian, L. Bingbing, *J. Physical chemistry.,* **(2012),** *116,* 11741

70. J. Zhenyuan, S. Xiaoping, L. Minzhi, Z. Hu, Z. Guoxing, C. Kangmin, *Nanotechnology.,* **(2013),** *24,*115603

71. S. Vaclav, B. Snejana, M.G. Tomas, B. Jana, K. Martin, *J. Chemistry Central.,* **(2013),** *7,* 41